Table 2
Compositions of infusion solution.

	g/500 ml												
	NaCl	KCl	$CaCl_2$	$MgCl_2$	$C_3H_5NaO_3$	$C_{12}H_{22}CaO_{14}$	K_2HPO_4	$MgSO_4$	ZnSO4	Amino acids	Glucose	pH	mequiv./L
Normal saline	4.50	–	–	–	–	–	–	–	–	–	–	6.0	1
AMINOFLUID®	0.39	–	–	–	1.15	0.41	0.56	0.31	0.70	15.00	37.50	6.7	3
AMICALIQ®	–	0.82	–	0.15	1.41	0.13	–	–	–	13.75	37.50	4.6–5.6	3
SOLITA®-T No. 3	0.45	0.75	–	–	1.12	–	–	–	–	–	21.5 0	3.5–6.5	1
Hartmann's solution pH 8	3.00	0.15	0.10	–	1.55	–	–	–	–	–		7.8–8.2	1
Lactec® Injection	3.00	0.15	0.10	–	1.55	–	–	–	–	–		6.0–8.5	0.9
MEYLON®	$NaHCO_3$	1.4 g/20 ml										7.0–8.5	5

ical Co., Inc., Tokyo, Japan) with a 10 m Teflon tube (0.5 mm i.d.) as a post-column. The automated pretreatment system consisted of a pretreatment column, a constant pump for cleaning solutions, and two switching valves. The pretreatment column used was a 2.5 cm stainless-steel (4.0 mm i.d.) 5 μm Ø LiChroCART 25-4 Lichrospher 100RP-18e (Merck, Darmstadt, Germany). The mobile phase consisted of acetonitrile:1/150 M phosphate-buffered solution (pH 6.3). The ratio of organic to aqueous phase was 28:72 (v/v). 1 M KOH was used for the reaction solution. Special grade ethanol (99.5%) was used for the cleaning solution. The flow rate of the mobile phase, reaction solution, and cleaning solution were 1.0 ml/min, 0.5 ml/min and 2.0 ml/min, respectively. The temperature of both columns was approximately 60 °C. A 50 μl aliquot of a two-fold diluted sample in mobile phase was injected. This system was constructed in accordance with the first supplement of the Japanese Pharmacopoeia (15th edition).

2.4.2. Dialysis method

Rate of PGE_1 retention in lipid particles was measured by a dialysis method. 340 μl of Lipo-PGE_1 was injected into a dialysis cassette, immersed in 85 ml of each infusion solution, and incubated with gentle agitation at 20 °C in a water bath. Each dialysis cassette was floated by using a buoy. After incubation for the indicated time the dialysis cassette was retrieved and the concentration of PGE_1 inside the cassette measured using the HPLC method described earlier. A 5 μg/ml solution of PGE_1 in normal saline was also injected into a dialysis cassette, incubated for the indicated time, and then the concentration of PGE_1 in the cassette measured as Lipo-PGE_1. The rate of PGE_1 retention was calculated in comparison with the 0 time sample, after correction for changes in volume of solution in the dialysis cassette.

3. Results and discussion

Firstly, we investigated whether the intravenous line becomes clogged by a suspention of generic Lipo-PGE_1 formulations and Hartmann's solution pH 8. A 2 ml solution of Formulation #1 (innovator) or Formulation #3 (generic) was injected into a 500 ml infusion bag of "Hartmann's solution pH 8." After mixing, an infusion set was attached to each infusion bag and the roller clamp was fully opened. In the suspension of Formulation #1, no decrease in drip rate or accumulation of aggregated substances in the infusion line was observed. By contrast, the drip rate of a suspension of Formulation #3 significantly decreased after 1 h and had completely stopped after 2 h. Additionally, a white aggregation substance was observed in the infusion line of the suspension of Formulation #3 (Fig. 1). Thus, we confirmed the previously reported phenomena.

We reasoned that an increase in the diameter of lipid particles in the infusion solution was likely to cause a decrease in the drop rate and the formation of aggregates. Therefore, after mixing of Lipo-PGE_1 with infusion solution, the time-dependent change in the mean diameter of lipid particles in the suspension was measured by dynamic light scattering (DLS) (Fig. 2). Seven different infusion solutions were used in this study as listed in Table 2. Hartmann's solution pH 8 and Ringer's lactate with sodium bicarbonate solution were included, which have been reported to cause aggregates and blockages in the infusion line. The mixing of Lipo-PGE_1 with Aminofluid® or Amicaliq® induced no obvious alteration in the size of the lipid particles over time, although the mean diameter was slightly greater compared to that observed using normal saline. The slightly greater diameter of the Lipo-PGE_1 particles in the presence of Aminofluid® or Amicaliq® is presumably caused by an accumulation of positively charged substances, such as arginine, histidine, Mg^{2+} and Zn^{2+}, around the lipid particle. In the case of Solita-T® No. 3 and Lactec® Injection, the mean diameter of the lipid particles was unchanged compared with that observed in normal saline. The mixing of Formulation #3 or Formulation #4 with the mixture of Lactec® injection and Meylon® (a 7% sodium bicarbonate injection) transiently increased the mean diameter of the lipid particles, although that of innovator formulations did not. Interestingly, there was no significant increase in the mean diameter of lipid particles in Hartmann's solution pH 8.

Next, the number of large diameter lipid particles was determined in suspensions of Lipo-PGE_1 in infusion solution using a single-particle optical sensing (SPOS) method. The number of lipid

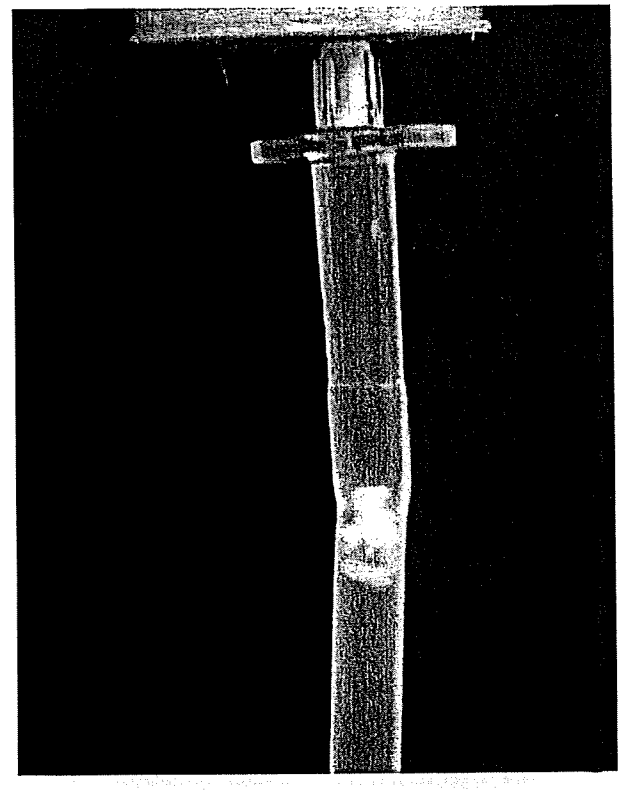

Fig. 1. Photograph of aggregation substances in suspension with Formulation #3 and Hartmann's solution pH 8.

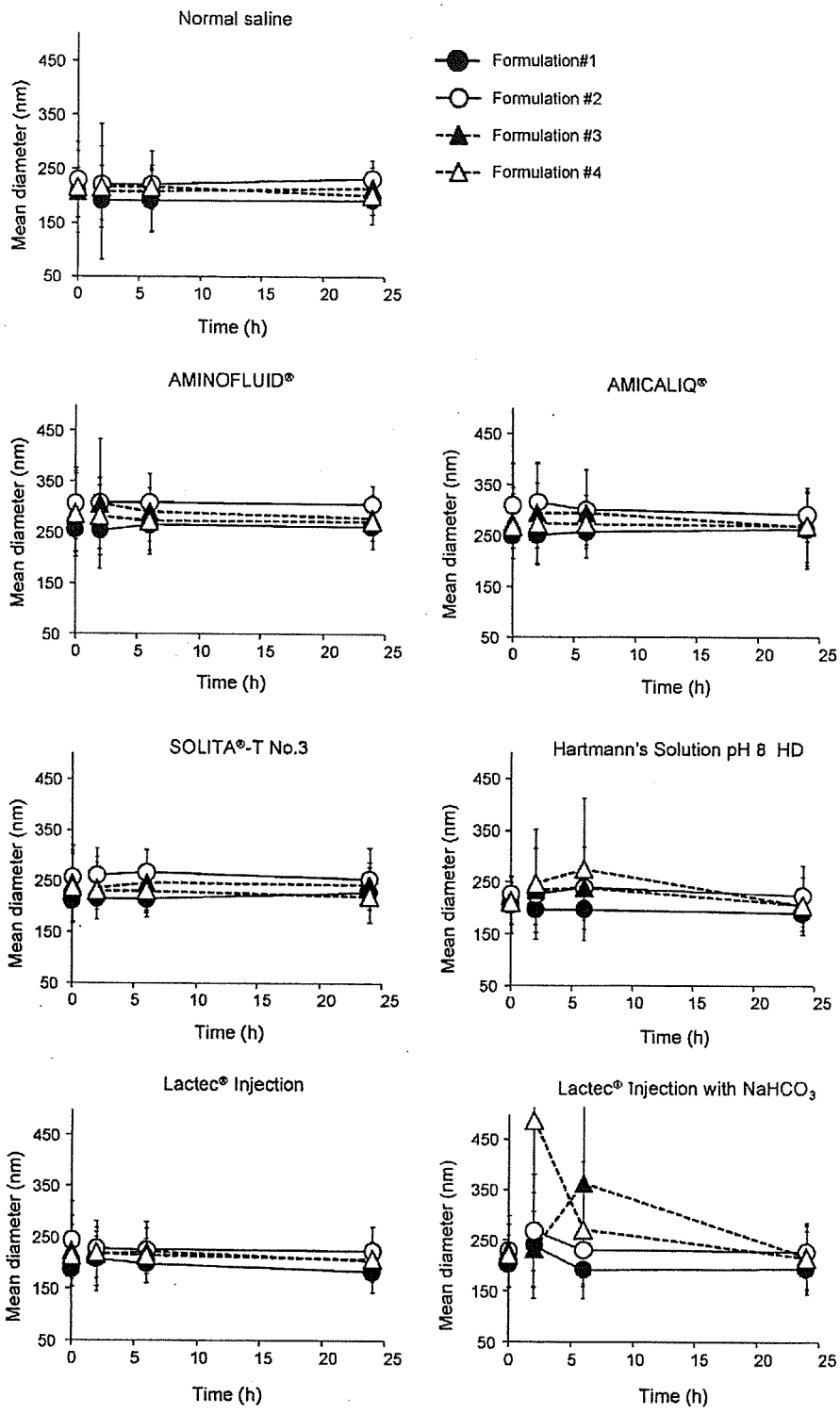

Fig. 2. Mean diameter of Lipo-PGE_1 after mixing with each infusion solution. Lipo-PGE_1 was mixed with each infusion solution and incubated at room temperature. Data represent the mean ± SD.

particles with a diameter >0.5 μm or >1 μm in an emulsion of Lipo-PGE_1 with each infusion solution is shown in Figs. 3 and 4, respectively. Intriguingly, the particle number >0.5 μm of generic formulations was larger than that of innovator formulations in all of the infusion solutions tested, while the particle number >1 μm of generic formulations was clearly smaller than that of innovator formulations in most of the infusion solutions, except Hartmann's solution pH 8 and Lactec® injection with Meylon®. Mixing generic formulations in Hartmann's solution pH 8 HD caused a significant increase in particle number especially with a diameter >1.0 μm. However, the particle number >1.0 μm of innovator formulations remained unchanged, although the particle number >0.5 μm of For-

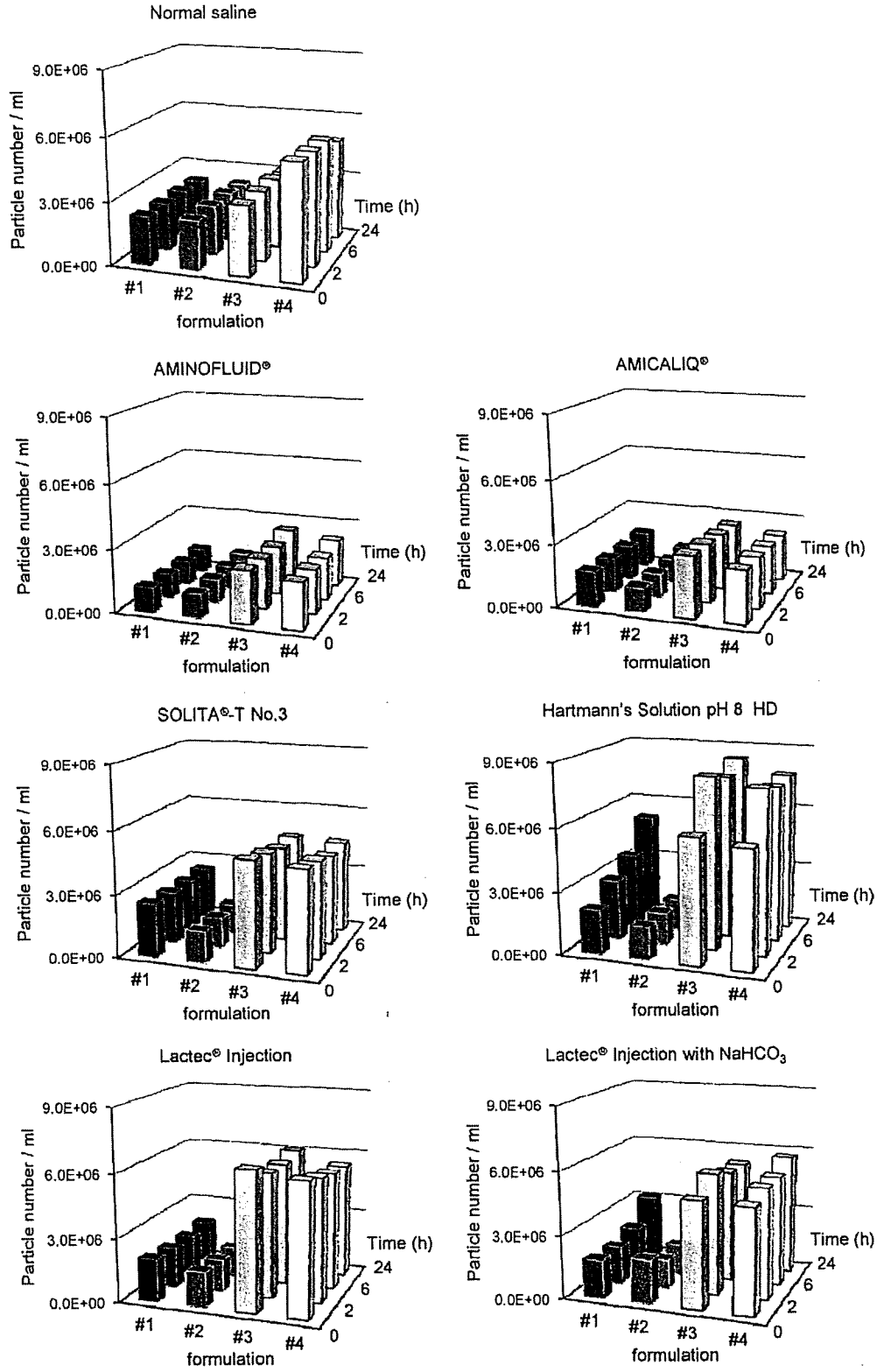

Fig. 3. Effect of each infusion solution on the total particle number of Lipo-PGE_1. The counts per milliliter per size range were normalized to the undiluted sample. Data represent the mean of two samples. Error bars were omitted by reason of the small standard deviations.

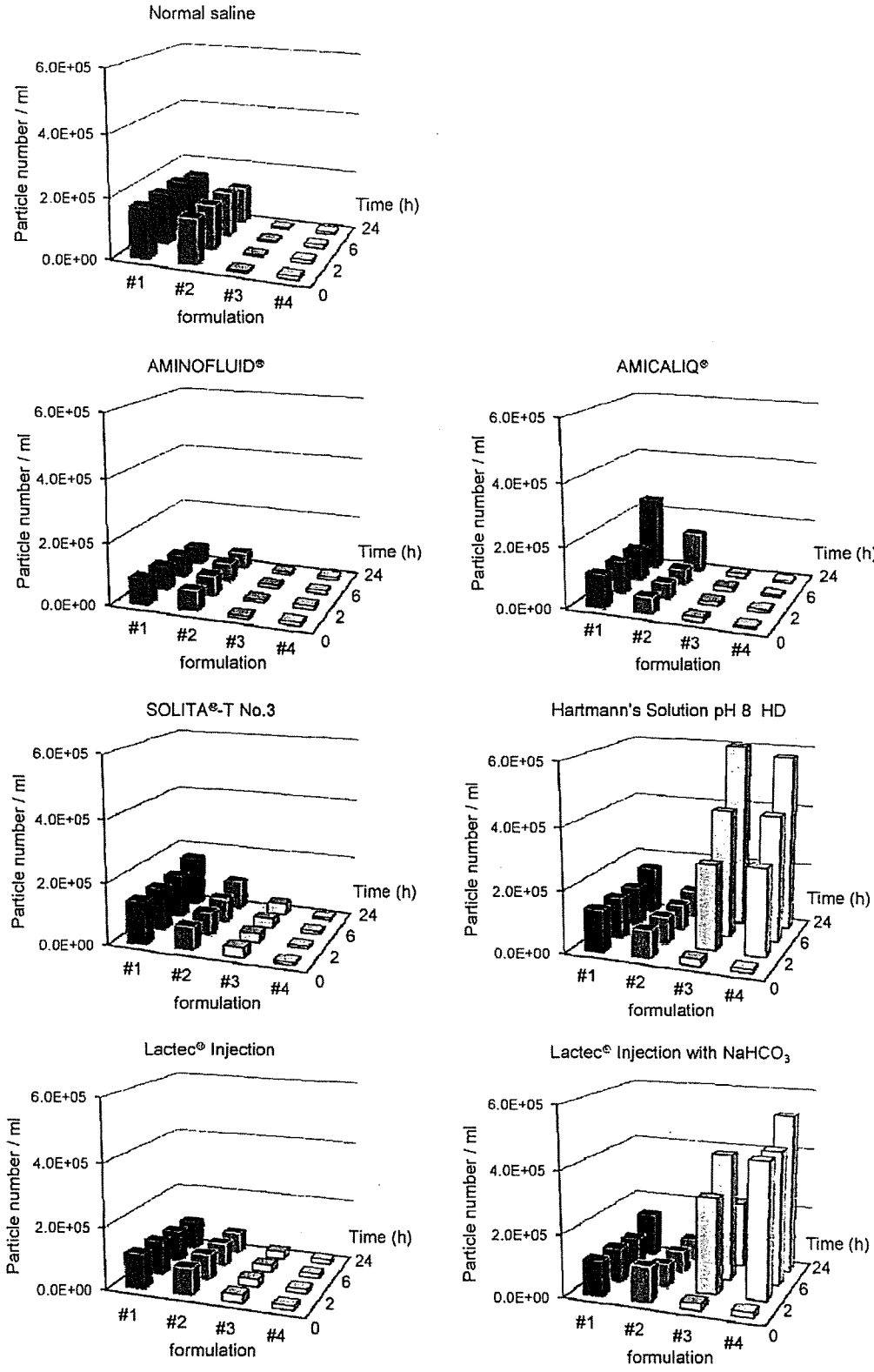

Fig. 4. Effect of each infusion solution on the large particle (diameter > 1.0 μm) number of Lipo-PGE_1.

mulation #1 gradually increased over time. Furthermore, in Lactec® injection with Meylon®, the particle number >1.0 μm of generic formulations increased markedly. Fig. 5 shows the particle distribution in an emulsion of each formulation with Hartmann's solution pH 8 or Lactec® injection with Meylon®. Among the innovator formulations, the distribution curve of Formulation #2 was unchanged, even 24 h after mixing, although that of Formulation #1 displayed an increase in the number of large particles. For the generic for-

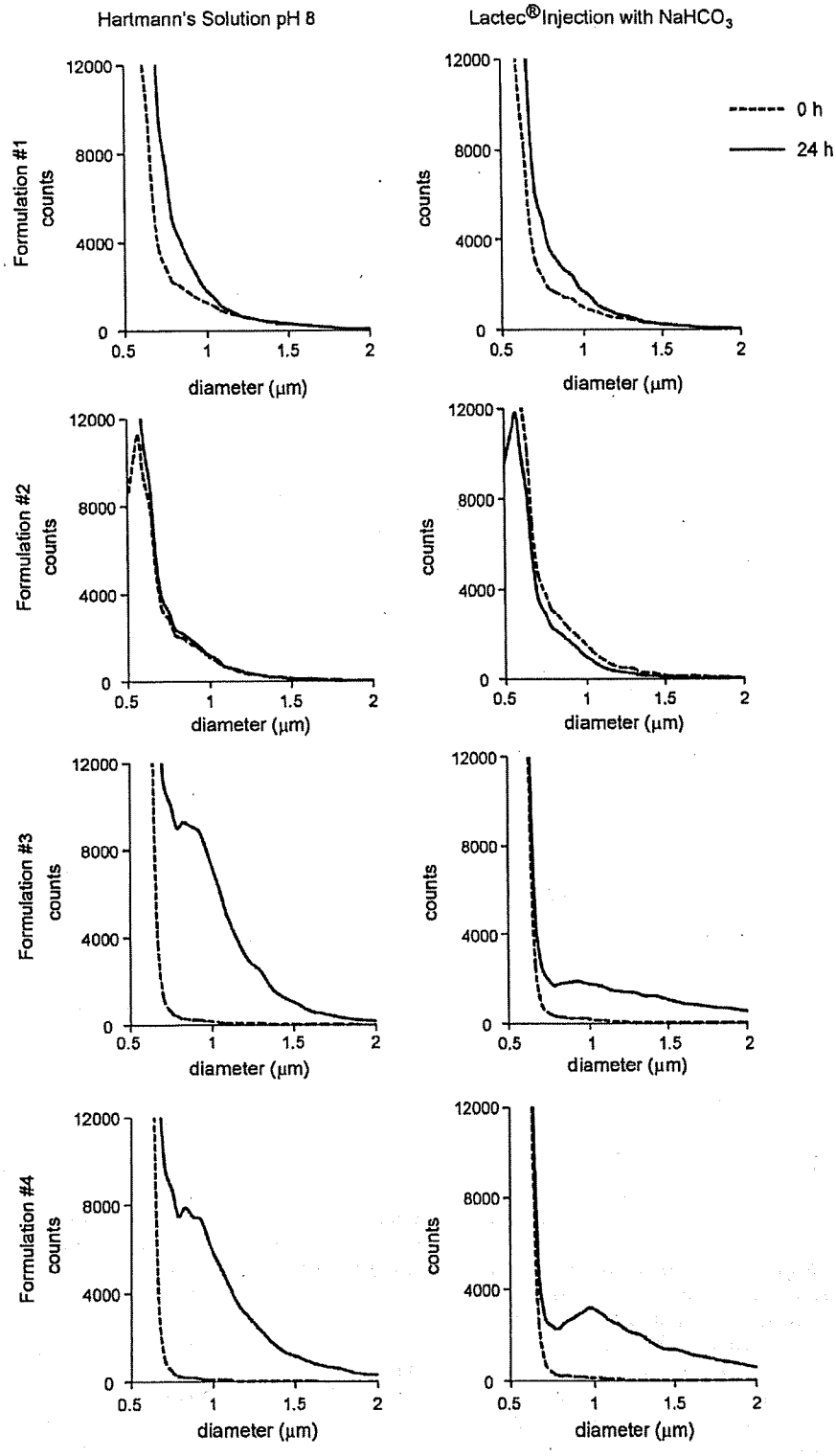

Fig. 5. distribution of Lipo-PGE_1 in Hartmann's solution pH 8 or Lactec® Injection with $NaHCO_3$. Dashed lines show 0 time, and full lines show 24 h after mixing with Lipo-PGE_1 and each infusion solution.

mulations, a significant increase of lipid particles of around 1 μm in diameter or a broad distribution of large particles was observed in Hartmann's solution pH 8 or Lactec® injection with Meylon®, respectively. These results indicate that the increase in the size of the lipid particles is related to the infusion solution used. The change in the size of the lipid particles in Amicaliq® was observed over a period of time. The particle number of innovator formulations increased 24 h after mixing, while that of generic formulations did not. In other infusion solutions there were no change in the particle number.

Table 3
Volume-weighted percentages of lipid particles with a diameter of >5 μm ($PFAT_5$) 2 h after suspension.

Lipo-PGE_1	Normal saline	Mean ± S.D.	
		Hartomann's solution pH 8 HD	Lactec® Injection with $NaHCO_3$
Formulation #1	0.025 ± 0.006	0.026 ± 0.002	0.009 ± 0.001
Formulation #2	0.006 ± 0.001	0.007 ± 0.001	0.007 ± 0.001
Formulation #3	0.034 ± 0.002	0.014 ± 0.004	0.056 ± 0.004
Formulation #4	0.012 ± 0.003	0.008 ± 0.001	0.012 ± 0.002

These results indicate that the substantial increase in the number of large particles is a potential factor leading to the aggregation of substances in the infusion line and slowing of the drip rate. Moreover, our studies revealed that, even using innovator formulations, the mixing of Formulation #1 with Hartmann's solution pH 8 increased the number of large particles at some level. Thus, in some cases, the SPOS method could detect changes in the number of large particles that could not be detected by the measurement of mean diameter or size distribution using DLS. Our data also indicate that the SPOS method may be a useful means of assessing the formulation stability of emulsions or the incompatibility with infusion solutions. Although the actual number of particles is given in this study, in USP ⟨729⟩, the instrument range of detection is set at 1.8–50 μm, and the volume-weighted percentage of lipid particles greater than 5 μm ($PFAT_5$) must be less than 0.05%. Thus, the $PFAT_5$ of each Lipo-PGE_1 formulation was calculated after mixing with normal saline, Hartmann's solution pH 8, or Lactec® injection with Meylon® (Table 3). Only the $PFAT_5$ of Formulation #3 in Lactec® injection with Meylon® was more than 0.05%, and the $PFAT_5$ of even generic formulations did not exceed 0.05%. This is because there was a significant increase in the number of lipid particles around 1 μm in diameter in the emulsion of generic formulations with Hartmann's solution pH 8. Such emulsion conditions could result in a blocked infusion line or at least some build-up of aggregation substances. Therefore, a measurement of the number of particles not only larger than 5 μm but also around 1 μm will be required depending on the particular situation. Large particles ranging from dozens to several hundred μm in diameter, which can clog the infusion line directly, were not detected in our study. There is a possibility that the partial accumulation of lipid particles around 1 μm may trigger a blockage in the infusion line. However, we could not eliminate the existence of large particles that are not detected by the SPOS method because they may be unstable in the very high flow rates used in this technique. Nevertheless, the assessment of emulsions using the SPOS method will simplify the procedure and allow the detection of a wide distribution of particle sizes.

One factor that may increase the number of large particles in the emulsion of generic Lipo-PGE_1 but not innovator Lipo-PGE_1 under alkaline conditions in the presence of calcium ions, such as Hartmann's solution pH 8 or Lactec® injection with Meylon®, is the zeta potential of the particle surfaces. As is well known, an electric charge on the particle surface brings about inter-particle repulsion, thereby preventing aggregation (Washington et al., 1989; Washington, 1990). If the electric charge of the particles in the emulsion is small, the stability of the emulsion will decrease. Thus, the zeta potential of each Lipo-PGE_1 formulation in water was measured (Table 4). Surprisingly, there were no significant differences between innovator and generic formulations. Indeed, the zeta potential of the generic formulations was slightly lower than that of the innovator formulations. This result indicates at least that the difference of zeta potential in normal saline may not be a factor causing the difference in stability between generic and innovator formulations under alkaline conditions in the presence of calcium ions. To clarify the effect of zeta potential on the formation of aggregation, the zeta potential value of each formulation in all infusion solutions as well as various pH solutions in the presence or absence of calcium ions should be measured as a subject of future investigation. Other factors include not only the difference in the method for manufacturing or the control of the process, but also a difference in the formulation. While the lipid particle of innovator formulations is composed of soybean oil, that of generic formulations is composed of olive oil as shown in Table 1. These two kinds of plant oil seem to have some differences in their physical characteristics because the main fatty acid of soybean or olive oil is linoleic acid or oleic acid, respectively. All additives in the generic formulations, except the oil, are exactly the same as innovator formulations. The hydrophile–lipophile balance (HLB) of emulsifier or oil as well as temperature and pH is important for the stability of the emulsion (Griffin, 1954; Becher, 1957). Thus, there is a possibility that the change of plant oil might bring about an alteration in the appropriate HLB of lecitin, and cause instability within the emulsion such as aggregation. Additionally, the HLB of lecitin is not constant like 7–13, because lecitin is a mixture of emulsifiers. Therefore, the HLB, relative proportion, or purity of lecitin might bring about the observed difference in stability. In either case, a detailed investigation will be required to reveal the cause of the increase in the number of large particles in generic formulations under alkaline conditions in the presence of calcium ions.

One report suggests that the PGE_1 retention rate of generic formulations in lipid emulsions is lower than that of the innovator formulations (Takenaga et al., 2007). Lipo-PGE_1 should be present at a high concentration within a lesion and maintain the concentration and activity of PGE_1 in the circulatory system. Stable retention of PGE_1 within the lipid particle is very important for exhibiting clinical effectiveness. Thus, the PGE_1 retention rate was measured in normal saline, Solita®-T No. 3, and the infusion solution in which the number of large particles increased, such as Amicaliq®, Hartmann's solution pH 8, and Lactec® injection with Meylon® (Fig. 6). The PGE_1 retention rates were measured using either the filtration, dialysis, or ultrafiltration method in previous reports (Takenaga et al., 2007; Igarashi et al., 1988; Yamaguchi et al., 1995; Teagarden et al., 1988). In the filtration method, the sample is passed through a membrane filter with a pore size of 0.1 μm connected to a disposable syringe. However, smaller particles may pass through the filter unit causing the data to fluctuate depending on the precise force applied to the syringe. In this study, the PGE_1 retention rate was measured by the dialysis method. Compared to a solution of PGE_1, each formulation clearly retained PGE_1 in lipid particles in normal saline, Solita®-

Table 4
Zeta potential of Lipo-PGE_1.

Peak position	Formulation #1 (innovator)	Formulation # 2 (innovator)	Formulation # 3 (generic)	Formulation # 4 (generic)
Mean (mV)	−23.1	−24.5	−29.5	−28.3
Width (mV)	6.0	7.1	6.1	4.9

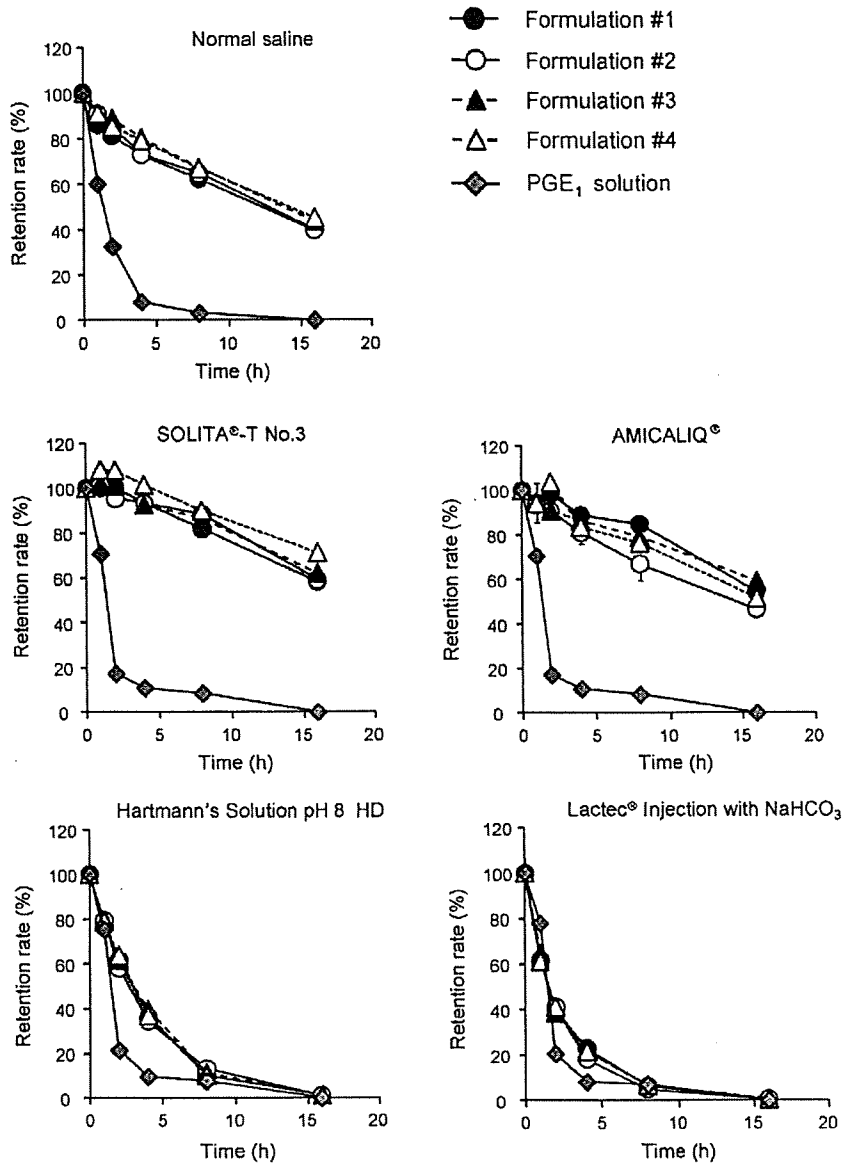

Fig. 6. Retention rate of PGE_1 in lipid particles in each infusion solution. Retention rate of PGE_1 in lipid particles of Lipo-PGE_1 was measured by the dialysis method at 20 °C. Plots show mean ± SD of percentages for three individual experiments. Solution PGE_1 (closed diamond) was used for a control of Lipo-PGE_1.

T No. 3 and Amicaliq® (Fig. 6). Moreover, there were no significant differences between formulations in these three infusion solutions. PGE_1 was rapidly released from lipid particles in Hartmann's solution pH 8, and Lactec® injection with Meylon®. Indeed, almost no PGE_1 remained in the lipid particles after 8 h. These results correlate with previous reports which indicated that the PGE_1 retention rate was influenced by the pH of buffered solution (Yamaguchi et al., 1995). This is because in alkaline condition PGE_1 (pK_a = 4.89) is anionic form and readily released from lipid particled while in acidic condition PGE1 is nutral form and mainly distributed to the oil/water interface (Teagarden et al., 1988). Even in these two infusion solutions, in which an increase in the number of large particles was observed, differences in the PGE_1 retention rate between innovator and generic formulations were not detected. Therefore, our results indicate that the PGE_1 retention rate of generic formulations is no lower than that of the innovator formulations.

Our study shows that the marked increase of large diameter (>1 μm) particles is a likely reason for the slowing of the drip rate and aggregation of substances in an infusion line of generic formulations under alkaline conditions in the presence of calcium ions. Moreover, our study indicates that a measurement of the number of large particles is very effective in assessing the stability of an emulsion. We also show that the mixing of Lipo-PGE_1 with Hartmann's solution pH 8 or Lactec® injection with Meylon® significantly decreased the retention rate of PGE_1 in lipid particles compared to normal saline. This decreased retention rate of PGE_1 is undesirable if Lipo-PGE_1 is to exert its full clinical effectiveness. Actually, the mixing of Lipo-PGE_1 with medicines other than infusion solution is restricted according to the package insert. However, the application of Hartmann's solution pH 8 is unrestricted because it is an infusion solution. Care must be taken over the choice of infusion solution due to the increase in the number of large particles generated using the generic formulations. Furthermore, it is preferable to administer Lipo-PGE_1 at as low a dilution as possible. In conclusion, except under alkaline conditions in the presence of calcium ions, there is no difference in mixing any infusion solu-

tion with Lipo-PGE_1. Specifically, there is no differences between generic formulations and innovator formulations in terms of PGE_1 retention rate in lipid particles. Thus the clinical effect of generic formulations will not differ greatly from that of innovator formulations.

References

Becher, P., 1957. Emulsions: Theory and Practice. Reinhold, New York, pp. 189–196.

Driscoll, D.F., Etzler, F., Barber, T.A., Nehne, J., Niemann, W., Bistrian, B.R., 2001. Physicochemical assessments of parenteral lipid emulsions: light obscuration versus laser diffraction. Int. J. Pharm. 219, 21–37.

Goto, N., Sakaya, H., Nakamura, T., Wakiya, Y., Masada, M., 2005. The 125th Annual Meeting of the Pharmaceutical Society of Japan 29-0816.

Golub, M., Zia, P., Matsuno, M., Horton, R., 1975. Metabolism of prostaglandins A1 and E1 in man. J. Clin. Invest. 56, 1404–1410.

Griffin, W.C., 1954. J. Soc. Cosmet. Chem. 5, 249.

Guyton, A.C., 1991. The microcirculation and the lymphatic system: capillary fluid exchange, interstitial fluid and lymph flow. In: Guyton, A.C. (Ed.), Textbook of Medical Physiology, 8th edn. Saunders, Philadelphia, pp. 170–184.

Igarashi, R., Nakagawa, M., Mizushima, Y., 1988. The bioactivity of esterified PGE1 and its application for lipid microspheres. Jpn. J. Inflamm. 8, 243–246.

Kramer, H.H., Sommer, M., Rammos, S., Krogmann, O., 1995. Evaluation of low dose prostaglandin E1 treatment for ductus dependent congenital heart disease. Eur. J. Pediatr. 154, 700–707.

Makita, S., Nakamura, M., Ohhira, A., Itoh, S., Hiramori, K., 1997. Effects of prostaglandin E1 infusion on limb hemodynamics and vasodilatory response in patients with arteriosclerosis obliterans. Cardiovasc. Drugs Ther. 11, 441–448.

Milio, G., Cospite, V., Cospite, M., 2003. Effects of PGE-1 in patients suffering from peripheral arterial occlusive disease. Minerva Cardioangiol. 51, 311–316.

Mizushima, Y., Hamano, T., Haramoto, S., Kiyokawa, S., Yanagawa, A., Nakura, K., Shintome, M., Watanabe, M., 1990. Distribution of lipid microspheres incorporating prostaglandin E1 to vascular lesions. Prostag. Leukot. Essent. Fatty Acids 41, 269–272.

Mizushima, Y., Yanagawa, A., Hoshi, K., 1983. Prostaglandin E1 is more effective, when incorporated in lipid microspheres, for treatment of peripheral vascular diseases in man. J Pharm. Pharmacol. 35, 666–667.

Otomo, S., Mizushima, T., Aihara, H., Yokoyama, K., Watanabe, M., Yanagawa, A., 1985. Prostaglandin E1 incorporated in lipid microspheres (Lipo PGE1). Drugs Exp. Clin. Res. 11, 627–631.

Sakaya, H., Goto, N., Nakamura, T., Wakiya, Y., Masada, M., 2005. The 125th annual meeting of the pharmaceutical society of Japan, 29-0815.

Schramek, P., Waldhauser, M., 1989. Dose-dependent effect and side-effect of prostaglandin E1 in erectile dysfunction. Br. J. Clin. Pharmacol. 28, 567–571.

Takenaga, M., Ohta, Y., Tokura, Y., Hamaguchi, A., Igarashi, R., 2007. Comparison study of lipo PGE1 preparations. Yakugaku Zasshi 127, 1237–1243.

Teagarden, D.L., Anderson, B.D., Petre, W.J., 1988. Determination of the pH-dependent phase distribution of prostaglandin E1 in a lipid emulsion by ultrafiltration. Pharm Res. 5, 482–487.

Yamaguchi, T., Fukushima, Y., Itai, S., Hayashi, H., 1995. Rate of release and retentivity of prostaglandin E1 in lipid emulsion. Biochim. Biophys. Acta 1256, 381–386.

Washington, C., Chawla, A., Christy, N., Davis, S.S., 1989. The electrokinetics properties of phospholipid-stabilized fat emulsions. Int. J. Pharm. 54, 191–197.

Washington, C., 1990. The stability of intravenous fat emulsions in total parenteral-nutrition mixtures. Int. J. Pharm. 66, 1–21.

Division of Drugs[1], National Institute of Health Sciences, Tokyo, Japan; TeraView Limited[2], St John's Innovation Park, Cambridge, United Kingdom; TDDS Research Laboratory[3], Hisamitsu Pharmaceutical Co. Inc., Tsukuba; Bruker Optics K.K[4], Tokyo, Japan

Detection of tulobuterol crystal in transdermal patches using Terahertz pulsed spectroscopy and imaging

T. Sakamoto[1], A. Portieri[2], P. F. Taday[2], Y. Takada[3], D. Sasakura[4], K. Aida[3], T. Matsubara[4], T. Miura[4], T. Terahara[3], D. D. Arnone[2], T. Kawanishi[1], Y. Hiyama[1]

Received January 19, 2009, accepted February 21, 2009

Dr. Tamoaki Sakamoto, Division of Drugs, National Institute of Health Sciences, 1-18-1, Kami-yoga, Setagaya-ku, Tokyo 158-8501, Japan
tsakamot@nihs.go.jp

Pharmazie 64: 361–365 (2009) *doi: 10.1691/ph.2009.9022*

Applicability of a Terahertz Pulsed Spectroscopy (TPS) and a Terahertz Pulsed Imaging (TPI) for detection of tulobuterol (TBR) crystals in transdermal patches was investigated. Because TBR has high permeability in dermis, crystalline TBR in patch matrices contributes to controlling the release rate of TBR from a matrix. Therefore, crystalline TBR is one of the important factors for quality control of TBR transdermal tapes. A model tape that includes 5 w/w%, 10 w/w%, 20 w/w% or 30 w/w% of TBR was measured by TPS/TPI. TBR crystals in the matrices were successfully detected by TPI. Identification of TBR in an image of a crystal-like mass was done by comparison between the spectra of tapes and a TBR standard substance. These results indicate that TPS and TPI are applicable to identifying crystalline lumps of an active drug in tapes for quality control.

1. Introduction

Terahertz (THz) time-domain spectroscopy gives an electric field record of time delay due to the presence of material in a beam path with a higher refractive index when compared to a reference. Fourier-transformed waveforms from an electric field show a characteristic relationship between frequency and absorbance. Fourier-transformed waveforms provide information about not only intra-molecular vibration and lattice vibration, but also intermolecular forces and hydrogen bonds.

In the pharmaceutical industry, applications of TPS and TPI for discrimination of polymorphs (Taday et al. 2003; Walther et al. 2003; Strachan et al. 2004, 2005; Zeitler et al. 2005, 2006, 2007, Day et al. 2006) and for detecting unique waveforms of APIs have been reported. Thus, these technologies are expected to be used for qualitative and/or quantitative analysis (Taday et al. 2003; Upadhya et al. 2003; Ueno et al. 2006; Zeitler et al. 2006). In particular, THz spectroscopy has been used for detecting foreign materials in samples and for measuring the thickness of coatings (Fitzgerald et al. 2005; Zeitler et al. 2006; Ho et al. 2007).

Tulobuterol ((*R,S*)-2-tert-butylamino-1-(2-chlorophenyl) ethanol, TBR) transdermal tapes are used to cure bronchial asthma as a bronchodilator (β_2-blocker). TBR is one of the suitable compounds for systemic transdermal formulation because it has very high permeability into the keratin layer. The release rate of TBR from the matrix is controlled by the formation of lumps of TBR crystals. For this reason, crystallization of TBR in a matrix is an important factor assuring the quality of this tape. However, verifying the crystallization of an active drug is difficult because TDDS tapes (or patches) generally have a sandwich-like structure with a matrix between a liner and a supporting board. Although release testing is often used to evaluate "releasability", which is one of the physico-chemical properties of an active drug in transdermal pharmaceuticals, releasability is not a suitable parameter for evaluating crystallization of an active drug. In order to compensate for this disadvantage, development of an alternative method by which to observe crystallization of an active drug in a matrix through a liner and/or a supporting board is needed. This manuscript describes the applicability of one of the innovative non-destructive analytical techniques, TPS and TPI, for quality evaluation of TDDS tapes.

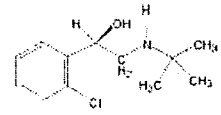

Tulobuterol

2. Investigations, results and discussions

2.1. THz pulsed spectrum of TBR obtained by TPS instrument

Fig. 1(A) shows the typical THz electric field records obtained from the TBR pellet and reference (PE pellet) by

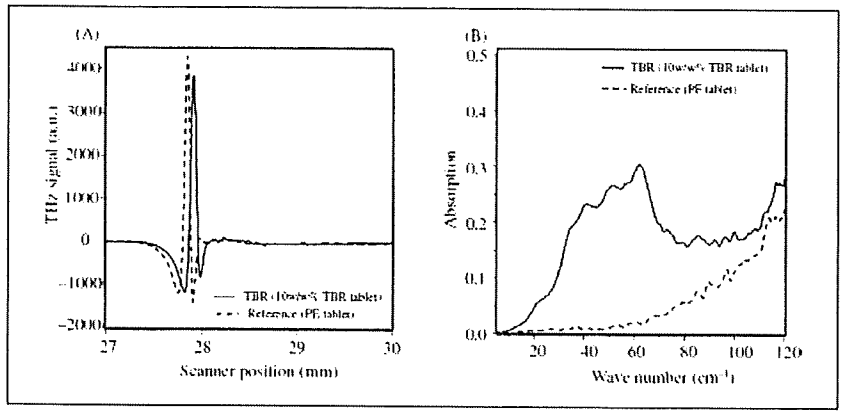

Fig. 1:
THz electric field records (A) and Fourier-transformed THz waveforms (B) of the TBR pellet and reference (PE pellet). The unique absorbance range, from 40 cm^{-1} to 70 cm^{-1}, is available to detect TBR absorbance

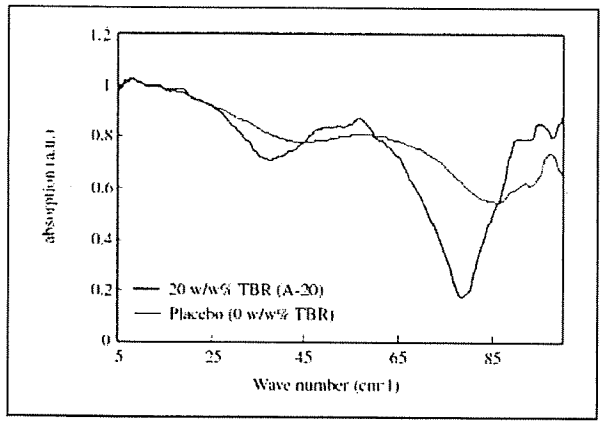

Fig. 2: THz spectra of model tape (20 w/w%, A-20) and placebo tape (0 w/w% TBR) obtained with quartz. The characteristic THz spectral range of TBR (from 45 cm^{-1} to 70 cm^{-1}) is best observed when etaloning effects are not dominating the range due to the thinness of the sample, as was the case here

the TPS 1000. The THz electric field record of the TBR pellet was shifted compared with that of the reference and the unique Fourier-transformed THz waveform of TBR was observed compared with that of the PE reference (Fig. 1(B)). This unique absorbance range, from 70 cm^{-1} to 45 cm^{-1}, seemed to be available to detect TBR absorbance from the total waveform of tapes.

2.2. *THz image and spectra of TBR crystal in matrix*

Fig. 2 shows the Fourier-transformed THz spectra of the placebo tape (the red line, an acrylic matrix) and the model tape (the blue line, 20w/w% TBR in an acrylic matrix, A-20). The fingerprint-like waveform of TBR from 70 cm^{-1} to 45 cm^{-1} was observed in the THz spectra obtained from the A-20. This observation suggests that chemical information of TBR can be detected in a tape. A lump of TBR crystals was detected at the top left of the image (Fig. 3(A)). The TPI contrast derives from refractive index differences. Therefore, it was presumed that the edge of the lumps of the TBR crystals contributed to making the definite contrast of shift of the refractive index. However, the image that is made from the shift of a refractive index would not provide chemical information about the lumps of TBR crystals. In order to identify the origin of the lumps of crystals, the THz spectra obtained from pixels which are located inside the lumps or outside the lumps were compared. Both spectra are shown in Fig. 3(B). The waveform indicated as the blue line represents the THz spectrum obtained from the pixel that is located inside the lump of crystals. The red line indicates the spectrum obtained from a pixel that is located outside the lump of crystals. The THz spectrum from the crystal shows a characteristic waveform range from 70 cm^{-1} to 45 cm^{-1}, almost the same as that of TBR standard substance. This observation strongly suggests that an image could be obtained from the crystal formed from TBR.

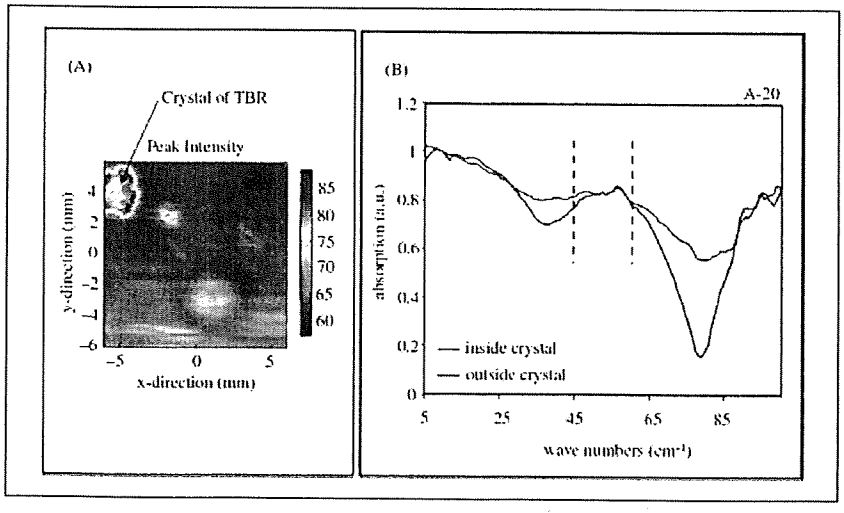

Fig. 3:
THz image of TBR crystal (A) and Fourier-transformed waveforms of pixels inside and outside of the crystals (B), obtained from A-20. The aggregation of TBR crystals which the arrow points to was clearly identified (A). It should be possible to observe the characteristic spectrum of TBR (from 45 cm^{-1} to 60 cm^{-1}) from both pixels located inside and outside of the crystal, but etaloning effects are again dominating the spectra

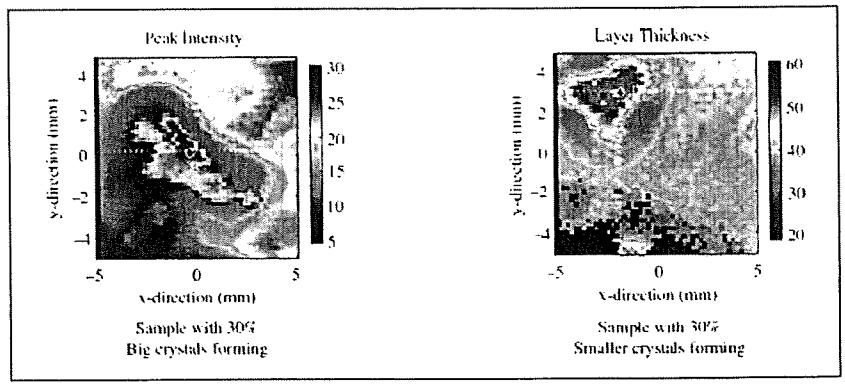

Fig. 4:
THz image of TBR crystals in matrix obtained using TPI 1000. Several sizes of TBR crystals were detected in the scanned area (the longer diameters: 0.5 mm to 3 mm, the shorter diameters: 0.1 mm to 0.2 mm)

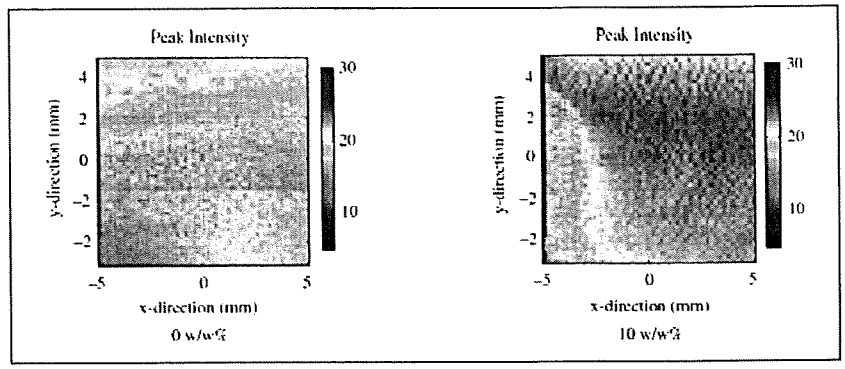

Fig. 5:
THz images of model tapes (0 and 10 w/w% TBR). Although there should be many small white crystals in R-10, only some were detected in the scanned area. In cases where the white crystals cannot be observed, the crystals might be smaller than the spatial resolution (100 μm) of TPI. Further studies need to be carried out to investigate differences in the samples

2.3. Size of crystals and spatial resolution of TPI

Fig. 4 shows the THz image obtained from the model tape (30 w/w% TBR, an acrylic matrix, A-30). Both model tapes were obtained from the same batch. Several sizes (short: 0.1 mm–0.2 mm, long: 0.5 mm–3 mm) of crystals were observed in these images.

The THz images obtained from the placebo tape (a rubber matrix, R-0) and the model tape (10 w/w% TBR, rubber matrix, R-10) are shown in Fig. 5. The image on the right side was obtained from R-10. Although small white crystals can be observed through a liner or a supporting board, no image of the lumps was observed in the THz image. This suggested that the sizes of the TBR crystals were smaller than the spatial resolution of TPI (approximately 100 μm). According to our study using Microscopic Laser Raman Spectroscopy/Mapping, the size of the TBR crystals was estimated to be from 6 μm to 40 μm (Sakamoto et al. 2006, 2007).

2.4. Depth image of crystals in TDDS tape

The THz image of A-30 and its depth image are shown in Fig. 6. The thickness of the lump of crystals in the matrix increased. The refractive index of the THz pulse was shifted due to the edges of the lumps of TBR crystals. This suggested that a comparatively big shift of a refractive index provides a definite image.

In conclusion, it was shown that THz spectroscopy/imaging technology was useful for detecting lumps of crystals of an active drug in transdermal tapes. THz spectroscopy/imaging can provide unique physical (and/or certain kinds of chemical) information compared with near infrared and/or mid infrared spectroscopy/imaging. In particular, obtaining a depth image from a pharmaceutical sample would be very useful for gaining an in-depth understanding of the quality of pharmaceuticals.

Although approximately 100 μm of spatial resolution in the THz pulsed image would hinder the detection of min-

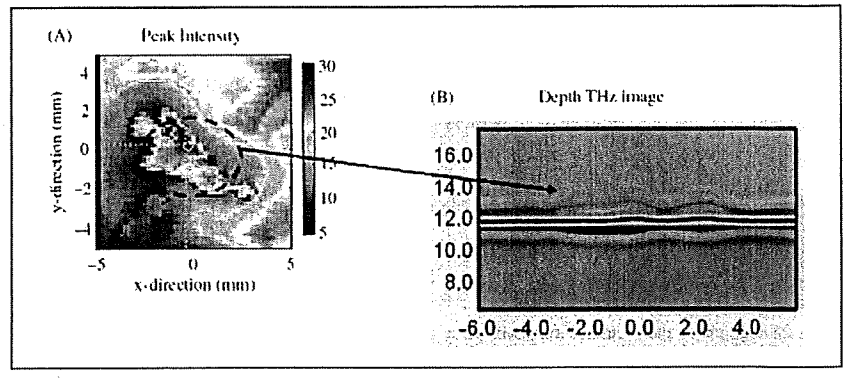

Fig. 6:
THz image of TBR crystal and depth THz image of matrix (A). The depth THz image in the scanned area where the crystal is observed shows the change in the thickness of the tape that can be seen (B)

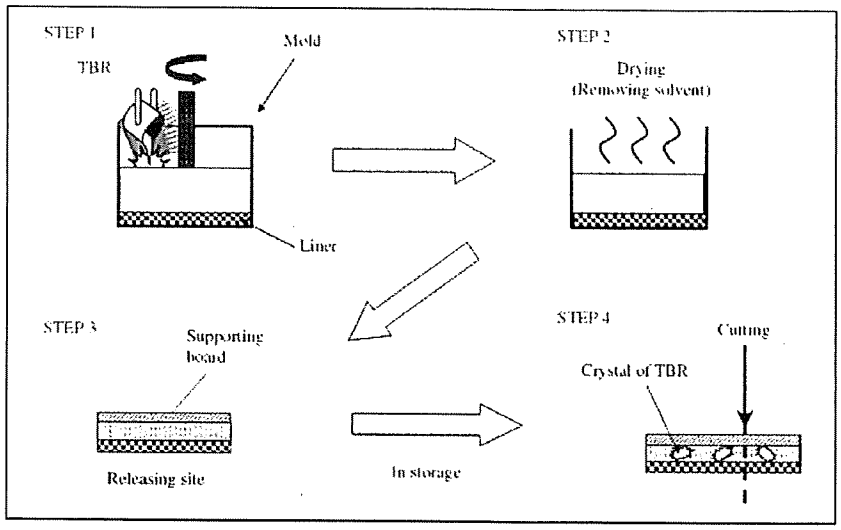

Fig. 7:
Flowchart showing preparation of model tapes. Residual solvents were removed by heating, and the mold was used to produce a sheet of model tape with a constant thickness and area

ute particles that are smaller than the spatial resolution, a reflective index of the THz pulsed wave may provide other useful information. Moreover, it would be able to detect problems caused by the manufacturing process, such as mixing of air bubbles and heterogeneity of active substances in the matrix. Therefore, this technology would be useful as an analytical tool not only for pharmaceutical quality control, but also for process control in pharmaceutical manufacturing.

Table: Prepared model transdermal tapes in this study

TBR level	Acrylic matrix	Rubber matrix
0 w/w% (Placebo)	A-0	R-0
10 w/w%	–	R-10
20 w/w%	A-20	–
30 w/w%	A-30	–

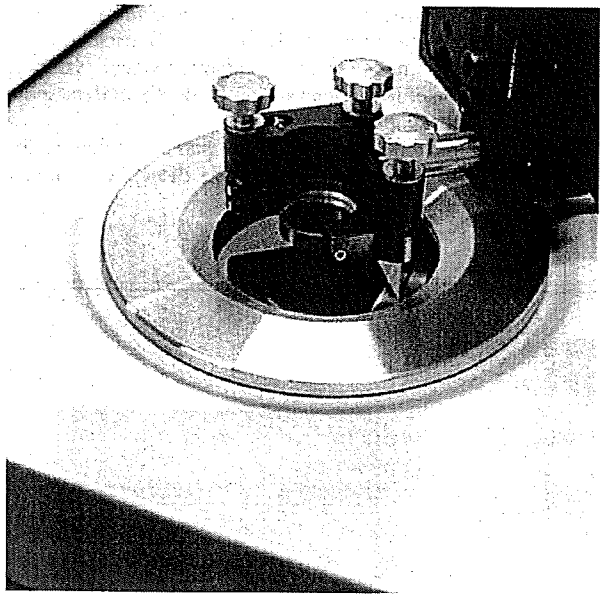

Fig. 8: Photograph of the metallic arm used when measuring the sample with a reference mirror

3. Experimental

3.1. Materials

TBR (purity > 99.0%) and model tapes were supplied by Hisamitsu Pharmaceutical Co Inc (Tokyo, Japan). Polyethylene (PE) powder of particle size < 80 µm was supplied by Induchem.

3.2. Model tapes

The model tapes were prepared by TDDS Laboratory, Hisamitsu Pharmaceutical Co Inc (Tsukuba, Japan). In order to identify crystals of TBR in the matrix, two kinds of matrices, rubber and acrylic matrices, were prepared. The flowchart for preparing the model tapes is shown in Fig. 7. TBR and other ingredients of the adhesive solutions were stirred in the mold adequately. The mixture was extended on the liner and residual solvents were removed by drying. When the thickness of the matrix (the adhesive layer) became a constant (approximately 50 µm thickness), a supporting board was pasted on the matrix after removing the mold. A polyethylene terephthalate (PET) film was selected as a liner and as a supporting board, for both the model and the placebo tape. And then these tapes cut to a size of 36 mm diameter. TBR crystals in model tapes were generated by leaving the tapes to crystallize for some time.
The model tape that contained 0 w/w% (R-0, placebo), 5 w/w% (R-5) or 10 w/w% (R-10) of TBR in a rubber matrix consisted of polyisobutylene, polybutene and lipocyclic petroleum resin. Small white crystals were seen in all areas of the matrix in the A-10 through a liner or a supporting board. The model tape that contained 0 w/w% (A-0, placebo), 20 w/w% (A-20) or 30 w/w% (A-30) of TBR in an acrylic matrix consisted of acryl adhesion polymer and isopropyl myristate. On the A-30 samples, small white crystals were seen in all areas of the matrices. A higher TBR concentration was needed to generate the crystals in the acrylic matrix compared with the rubber matrix because of the solubility of TBR. The prepared model tapes are shown in the Table.

3.3. Apparatus and measurements

3.3.1. Transmittance measurement of tablet by TPS

In order to identify a THz spectrum of TBR, a pellet containing approximately 10 w/w% of TBR was prepared by compressing at 2 t for 3 min with a press machine. The pellet was measured using a TPS 1000 spectrometer (TeraView Limited, Cambridge, UK). Each sample was measured covering the spectral range from 120 cm^{-1} to 2 cm^{-1} at 1.5 cm^{-1} of spectral resolution. Spectra were obtained averaging 1800 scans.

3.3.2. Transmittance-reflectance measurements of tapes by TPI

A reference mirror was first measured, and then the samples were mounted to the mirror and adjusted horizontally against the measurement window of the TPI Imaga™ 1000 instrument (Fig. 8); subsequently, THz radiation was focused onto the samples to gain maximum sensitivity. Placebo tapes were used as a background for all measurements.
A TPI imaging system, TPI Imaga 1000 (TeraView Ltd., Cambridge, UK), was used for the reflectance measurement, which was operated in the rapid scan mode. Terahertz images were obtained by raster scanning the terahertz beam across the sample, which was mounted at the focus position. The scanned area was 12 mm × 12 mm, which corresponds to 120 pixels × 120 pixels at 100 µm spatial resolution. The total measurement time was approximately 30 min.

Acknowledgement: This study was supported in part by a research grant from the Ministry of Health, Labour and Welfare of Japan (H17-iyaku-ippan-040).

References

Day GM, Zeitler JA, Jones W, Rades T, Taday PF (2006) Understanding the influence of polymorphism on phonon spectra: Lattice dynamics calculations and terahertz spectroscopy of carbamazepine. J Phys Chem B 110: 447–456.

Fitzgerald AJ, Cole BE, Taday PF (2005) Nondestructive analysis of tablet coating thicknesses using terahertz pulsed imaging. J Pharm Sci 94: 177–183.

Ho L, Müller R, Römer M, Gordon KC, Heinämäki J, Kleinebudde P, Pepper M, Rades T, Shen YC, Strachan CJ, Taday PF, Zeitler JA (2007) Analysis of sustained-release tablet film coats using terahertz pulsed imaging. J Control Release 119: 253–261.

Sakamoto T, Fujimaki Y, Hiyama Y (2007) Study on development of quality analytical method using spectroscopic and imaging technique I. Application of Raman spectroscopy and mapping microscopy for quality evaluation of TDDS and Granules formulations. PharmTech Japan 23: 27–36 (in Japanese).

Sakamoto T, Matsubara T, Sasakura D, Takada Y, Fujimaki Y, Aida K, Miura T, Terahara T, Higo N, Kawanishi T, Hiyama Y (2009) Chemical mapping of tulobuterol in transdermal tapes using Microscopic Laser Raman Spectroscopy. Pharmazie 64: 166–171.

Strachan CJ, Taday PF, Newnham DA, Gordon KC, Zeitler JA, Pepper M, Rades T (2005) Using terahertz pulsed spectroscopy to quantify pharmaceutical polymorphism and crystallinity. J Pharm Sci 94: 837–846.

Strachan CJ, Rides T, Newnham DA, Gordon KC, Pepper M, Taday PF (2004) Using terahertz pulsed spectroscopy to study crystallinity of pharmaceutical materials. Chem Phys Lett 390: 20–24.

Taday PF, Bradley IV, Arnone DD, Pepper M (2003) Using terahertz pulse spectroscopy to study the crystalline structure of a drug: a case study of the polymorphs of ranitidine hydrochloride. J Pharm Sci 92: 831–838.

Ueno Y, Rungsawang R, Tomita I, Ajito K (2006) Quantitative measurements of amino acids by terahertz time-domain transmission spectroscopy. Anal Chem 78: 5424–5428.

Upadhya PC, Shen YC, Davies AG, Linfield EH (2003) Terahertz time-domain spectroscopy of glucose and uric acid. J Biol Phys 29: 117–121.

Walther M, Fischer BM, Jepsen PU (2003) Noncovalent intermolecular forces in polycrystalline and amorphous saccharides in the far infrared. Chem Phys 288: 261–268.

Zeitler JA, Newnham DA, Taday PF, Strachan CJ, Pepper M, Gordon KC, Rades T (2005) Temperature dependent terahertz pulsed spectroscopy of carbamazepine. Thermochim Acta 436: 70–76.

Zeitler JA, Shen YC, Baker C, Taday PF, Pepper M, Rades T (2006) Analysis of coating structure and interfaces in solid oral dosage forms by three dimensional terahertz pulsed imaging. J Pharm Sci 96: 330–340.

Zeitler JA, Newnham DA, Taday PF, Threlfall TL, Lancaster RW, Berg RW, Strachan CJ, Pepper M, Gordon KC, Rades T (2006) Characterization of temperature-induced phase transitions in the five polymorphic forms of sulfathiazole by terahertz pulsed spectroscopy and differential scanning calorimetry. J Pharm Sci 95: 2486–2498.

Zeitler JA, Taday PF, Pepper M, Rades T (2007) Relaxation and crystallization of amorphous carbamazepine studied by terahertz pulsed spectroscopy. J Pharm Sci 96: 2703–2709.

Stabilization of Protein Structure in Freeze-Dried Amorphous Organic Acid Buffer Salts

Ken-ichi IZUTSU,*[,a] Saori KADOYA,[b] Chikako YOMOTA,[a] Toru KAWANISHI,[a] Etsuo YONEMOCHI,[b] and Katsuhide TERADA[b]

[a] *National Institute of Health Sciences; 1–18–1 Kamiyoga, Setagaya-ku, Tokyo 158–8501, Japan: and* [b] *Faculty of Pharmaceutical Sciences, Toho University; 2–2–1 Miyama, Funabashi, Chiba 274–8510, Japan.*

Received May 6, 2009; accepted August 5, 2009; published online August 6, 2009

The purpose of this study was to elucidate the physical properties and protein-stabilizing effects of some pH-adjusting excipients (carboxylic acids and their sodium salts) in frozen solutions and in freeze-dried solids. Thermal and powder X-ray diffraction (XRD) analysis indicated a high propensity of sodium citrates to form glass-state amorphous solids upon freeze-drying. Some salts (*e.g.*, sodium succinate) crystallized in the single-solute frozen solutions. FT-IR analysis of bovine serum albumin (BSA) and bovine immunoglobulin G (IgG) in the aqueous solutions and the freeze-dried solids showed that some glass-forming salts (*e.g.*, monosodium citrate) protected the secondary structure from lyophilization-induced perturbation. Freeze-drying of BSA at different concentrations indicated retention of the secondary structure at similar monosodium citrate/protein concentration ratios, suggesting stabilization through direct interaction that substitute water molecules inevitable for the conformation integrity. The carboxylic acid salts should provide rigid hydrogen bonds and electrostatic interactions that raise the glass transition temperature of the amorphous solids and stabilize protein structure. The relevance of the structural stabilization to the protein formulation design was discussed.

Key words freeze-drying; protein formulation; stabilization; glass; Fourier transform infrared spectroscopy

The development of protein pharmaceuticals requires rational formulation design to ensure appropriate storage stability, because the degradation of such pharmaceuticals through various chemical and physical pathways not only reduces their therapeutic effects but also increases the risk of product immunogenicity.[1—5] Freeze-drying is a popular method of conferring long-term stability of therapeutic proteins that is not achievable in aqueous solutions. Removal of the surrounding water molecules during the freeze-drying process, however, often perturbs the protein structure, leading to irreversible aggregation in the reconstituted solutions. The structurally altered protein molecules are also prone to chemical degradation during storage.[1] Maintaining the protein conformation by process and ingredient (*e.g.*, stabilizer, pH buffer, isotonic agents) optimization thus improves both the physical and chemical stability of protein formulations.

Choosing the solution pH and buffer system appropriate to a particular protein is a simple but significant element in the formulation design because the chemical and physical integrity of proteins in the aqueous solutions and freeze-dried solids depend largely on the pH.[6] Some buffer components also favorably or adversely affect the protein stability through direct interactions and/or through changing the local environments in the dried state. For example, freezing of certain buffer systems (*e.g.*, sodium phosphate) often induces crystallization of a component salt and resulting shift of the local pH surrounding the proteins.[7—11] Freeze-drying from some buffer systems (*e.g.*, L-histidine, citrate, or Tris) often leads to higher activity retention of proteins (*e.g.*, coagulation factor VIII, recombinant human interleukin-1 receptor antagonist) relative to those from other buffers.[12—15] Conformation of the proteins lyophilized in these buffer systems is of particular interest.

Reported properties of some carboxylic acid salts, including stabilization of native protein conformation in aqueous solutions (*e.g.*, antithrombin III)[16,17] and their propensity to form glass-state amorphous solids upon lyophilization,[18] suggest their ability to protect protein conformation against dehydration stress through mechanisms similar to disaccharides. Non-reducing disaccharides (*e.g.*, sucrose, trehalose) are popular stabilizers in solution and freeze-dried protein formulations. Various saccharides and polyols thermodynamically favor native protein structures over denatured states in aqueous solutions by a "preferential exclusion" mechanism.[19] Sucrose and trehalose protect proteins by substituting surrounding water molecules through hydrogen bonds during the freeze-drying process.[4,20—22] Limited molecular mobility in glass-state lyophilized disaccharide solids also protects embedded proteins from chemical degradation (*e.g.*, deamidation) during storage.[23]

The present study assesses the physical properties and protein-stabilizing effects of carboxylic acid buffer systems (*e.g.*, sodium citrate, sodium L-tartrate, sodium succinate) and their constituting salts against lyophilization-induced protein secondary structure changes. The physical properties of the frozen solutions and freeze-dried solids were studied by powder X-ray diffraction and thermal analysis. The effects of carboxylic acids and their sodium salts on the structural integrity of model proteins rich in α-helices [bovine serum albumin (BSA)] or β-sheets [bovine immunoglobulin G (IgG)], both prior to and after the freeze-drying process, were studied by Fourier transform infrared (FT-IR) spectroscopy of the amide I band combined with a mathematical band-narrowing technique (second-derivative).[24] Possible mechanisms of structural stabilization and their implications for formulation design are discussed.

Experimental

Materials Bovine serum albumin (A-7511, fatty acid content: approximately 0.005%, pI: 4.9), dextran 10.2k, and bovine immunoglobulin G (#64140) were purchased from Sigma-Aldrich Co. (St. Louis, MO, U.S.A.) and ICN Biomedicals Inc. (Aurora, OH, U.S.A.), respectively. Disodium hydrogen citrate sesquihydrate, monosodium citrate, and disodium(+)-tartrate dihydrate were obtained from Kanto Chemical Co. (Tokyo, Japan). Sodium

* To whom correspondence should be addressed. e-mail: izutsu@nihs.go.jp

hydrogen L-tartrate was purchased from Alfa Aesar GmbH & Co KG (Karlsruhe, Germany). Citric acid monohydrate, trisodium citrate dihydrate, sodium hydrogen L-tartrate, and other chemicals were purchased from Wako Pure Chemical, Co. (Osaka, Japan). The proteins were dialyzed overnight against buffer solutions (20 mM sodium phosphate, sodium citrate, sodium L-tartrate, sodium succinate, pH 6.0) using cellulose tubing (MWCO 14,000, Viskase Co., Darien, IL,U.S.A.). The dialyzed protein solutions were centrifuged (1500×*g*) and filtered (0.45 μm PVDF, Millipore, Bedford, MA, U.S.A.) before the freeze-drying study. Precipitation during dialysis reduced the IgG concentrations to 15—20 mg/ml in the resulting solutions. Monosodium succinate solution was prepared by mixing equivalent amounts of succinic acid and disodium succinate.

Freeze-Drying Freeze-drying was performed using a Freezone-6 lyophilizer equipped with temperature-controlled trays (Labconco, Kansas City, MO, U.S.A.). Aqueous solutions containing protein (10, 50 mg/ml) and various concentrations of excipients in flat-bottom glass vials (300 μl, 13 mm diameter) were placed on the shelf of the freeze-drier at room temperature. Some of the samples also contained low concentrations (1.5—10 mM) of the corresponding buffer system salts that were originally in the dialyzed protein stock solutions. The shelf was cooled to −40 °C at 0.5 °C/min and then maintained at this temperature for 2 h before the primary drying process. The frozen solutions were dried under vacuum (21 mTorr), with the shelf temperature maintained at −40 °C for 15 h, −30 °C for 6 h, and 35 °C for 6 h. The shelf was heated at a rate of 0.2 °C/min between the drying steps. The vials were sealed with rubber closures under vacuum. A pH meter (D-51, Horiba Ltd., Kyoto, Japan) and an electrode (9669-10D) were used to measure the pH values of solutions containing protein (*e.g.*, BSA) and excipients. The pH values of other solutions were obtained using a pH meter (HM-60G, TOA-DKK Co., Tokyo).

Thermal Analysis Thermal analysis of frozen solutions and dried solids was carried out using a differential scanning calorimeter (Q-10, TA Instruments, New Castle, DE, U.S.A.) and software (Universal Analysis 2000, TA Instruments). Aliquots of aqueous solutions (10 μl) in aluminum cells were cooled from room temperature at 10 °C/min and then scanned from −70 °C at 5 °C/min. Freeze-dried solids (0.5—1 mg) in hermetic aluminum cells were subjected to thermal analysis from −30 °C at 5 °C/min under nitrogen gas flow. Maximum inflection points in the heat flow discontinuities were assigned as glass transitions of maximally freeze-concentrated phases in frozen solutions (T_g') and glass transitions of freeze-dried solids (T_g).

Powder X-Ray Diffraction (XRD) Analysis Powder X-ray diffraction patterns were obtained at room temperature using a Rint-Altima diffractometer (Rigaku, Tokyo, Japan) with Cu$K\alpha$ radiation at 40 kV/50 mA. The samples were scanned through the range $5° < 2\theta < 35°$ at an angle speed of 5 °/min.

Measurement of Residual Water The amount of water in the freeze-dried solids suspended in dehydrated methanol was determined by the Karl–Fischer method using an AQV-6 volumetric titrator (Hiranuma Sangyo, Ibaraki, Japan).

Fourier-Transform Infrared Spectroscopy (FT-IR) The secondary structures of proteins were analyzed using an FT-IR system (MB104 spectrophotometer (ABB Bomen, Quebec, Canada) with PROTA (Bomen/Vysis) and GRAMS/32 (Galactic Ind. Co.) software. Transmission spectra of freeze-dried proteins were obtained from 256 scans of pressed disks containing freeze-dried solids (approx. 1 mg protein) and potassium bromide (approx. 250 mg) at a resolution of 4 cm^{-1}. Spectra of aqueous protein solutions (10 mg/ml) were recorded from 512 scans using an infrared cell with CaF_2 windows and a film spacer (6 μm). Reference spectra were recorded with the corresponding buffer and excipient solutions to obtain the absorbance spectra using an automated subtraction algorithm in PROTA. The second-derivative spectra obtained with the Savitski–Golay derivative function (7-point smoothing) were baseline-corrected and area-normalized in the amide I region (1600—1715 cm^{-1}).[25,26]

Results

The physical properties of organic acids and their sodium salts are summarized in Table 1. Thermal analysis indicated varied propensities of the excipients to crystallize in the frozen solutions. Frozen monosodium L-tartrate solution showed two exotherm peaks that indicate eutectic crystallization. Pairs of exothermic and endothermic peaks indicated eutectic solute crystallization and subsequent melting in the frozen mono- and disodium succinate solutions. A flat thermogram in the heating scan suggested crystallization of succinic acid in the cooling process. Other frozen excipient solutions showed thermal transition of the freeze-concentrated non-ice phase at certain temperatures (T_g': glass transitions of maximally freeze-concentrated phases).[4,27] Physical properties of some frozen buffer solutions (50 mM, pH 6.0) reflected those of the constituent salts. Frozen sodium citrate and sodium L-tartrate buffer solutions showed T_g' at −41.6 and −39.7 °C, respectively. In contrast, eutectic crystallization of their constituent salts resulted in an exotherm peak (−28.8 °C) and an endotherm peak (−9.6 °C) in the frozen sodium succinate buffer. The addition of BSA (10 mg/ml) and accompanying small amount of the buffer components (1.5 mM, pH 6.0) reduced the pH variation of the aqueous excipient (50 mM) solutions. A higher transition temperature (T_g') and the eutectic crystallization temperatures suggested reduced mobility of solute molecules in the freeze-concentrated mixture with BSA.[8]

Figure 1 shows thermograms of freeze-dried excipient solids. Heating scans of cake-structure freeze-dried monosodium L-tartrate, succinic acid, and monosodium succinate solutions

Table 1. Physical Properties of Carboxylic Acid and Their Sodium Salts

Excipients[a]	Frozen solutions				Freeze-dried solids		
	w/o BSA		with 10 mg/ml BSA		with 10 mg/ml BSA		
	pH	Thermal property	pH	Thermal property	Crystallinity[b]	Thermal property	Residual water (%)
Na_3-citrate	8.51	T_g': −43.0±1.2 °C	7.06	T_g': −35.8±0.1 °C	Amorphous	T_g: 74.9±2.0 °C	5.2±0.9
Na_2H-citrate	5.28	T_g': −39.1±0.0 °C	5.30	T_g': −31.6±0.2 °C	Amorphous	T_g: 78.2±2.6 °C	5.1±0.9
NaH_2-citrate	3.72	T_g': −33.2±0.2 °C	3.97	T_g': −24.4±1.1 °C	Amorphous	T_g: 61.1±1.8 °C	5.2±0.0
Citric acid	2.29	T_g': −55.0±0.3 °C	2.63	n.d.	Amorphous	T_g: 43.7±1.8 °C	5.5±1.8
Na_2-L-tartrate	7.24	T_g': −40.0±0.1 °C	6.73	T_g': −32.6±0.1 °C	Amorphous	T_g: 68.8±2.6 °C	4.9±2.1
NaH-L-tartrate	3.50	Exotherm: −26.2, −15.0 °C	3.72	Exotherm: −10.9 °C	Amorphous	T_g: 56.6±3.8 °C	7.0±2.2
L-Tartric acid	2.26	T_g': −56.6±0.8 °C	2.56	n.d.	Amorphous	T_g: 43.7±1.8 °C	8.4±0.4
Na_2-succinate	8.00	Exotherm: −36.6 °C Endotherm: −7.8 °C	6.90	Exotherm: −21.3 °C Endotherm: −8.4, −6.0 °C	Amorphous	n.d.	5.3±1.1
NaH-succinate[c]	4.73	Exotherm: −25.0 °C Endotherm: −8.1 °C	4.81	T_g': −39.5±0.7 °C Endotherm: −7.9 °C	Amorphous	T_g: 49.2±3.7 °C	7.7±1.2
Succinic acid	2.82	Unclear	3.41	Exotherm: −17.6 °C	Amorphous	T_g: 42.0±6.2 °C	6.0±1.3

a) 50 mM. *b*) Obtained by powder X-ray diffractometry. *c*) Prepared by mixing and disodium succinate and succinic acid.

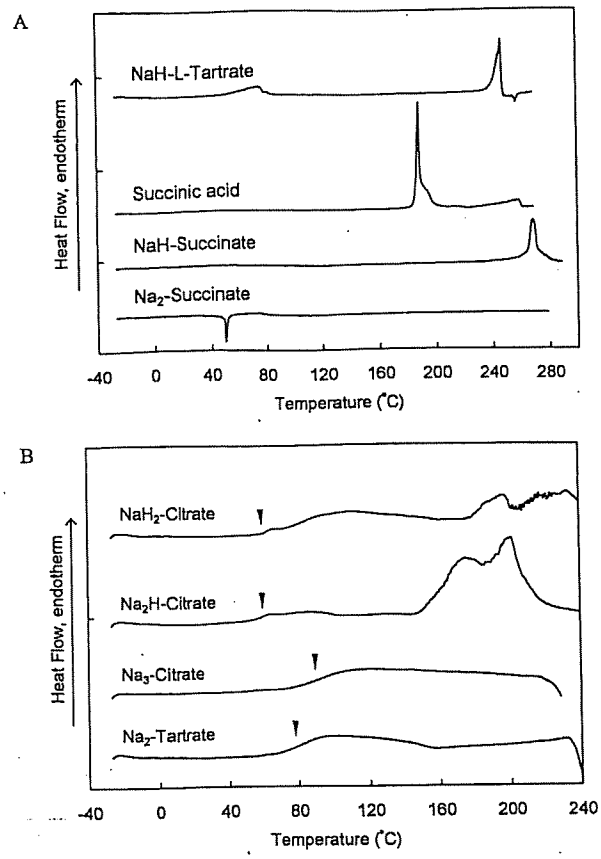

Fig. 1. Thermograms of Freeze-Dried Excipients (0.5—1 mg, 50 mM in Initial Solutions) Scanned from −30 °C at 5 °C/min

The solids presenting crystallization or melting peaks (A) and glass transitions (B) are shown at different heat flow scales. Arrowheads denote glass transitions of the freeze-dried solids (T_g).

(50 mM) showed endotherm peaks that indicate melting of the crystalline moiety (Fig. 1A). A crystallization exotherm at approximately 50 °C indicated the existence of an amorphous region in the freeze-dried disodium succinate solid. Frozen citric acid and L-tartaric acid solutions collapsed during the primary drying process, presumably because their T_g's were lower than the product temperature. Some diffraction peaks in powder X-ray diffraction patterns suggested partial crystallization of succinic acid and some salts (monosodium L-tartrate, disodium succinate) lyophilized in the absence of the protein (Fig. 2, some data not shown). Other organic acid salts formed glass-state amorphous solids during freeze-drying (Fig. 1B).

Co-lyophilization of the excipients (50 mM) with BSA (10 mg/ml) resulted in cylindrical cake-structure solids. Powder X-ray diffraction (XRD) analysis of the freeze-dried solids showed halo patterns that indicate largely amorphous components (Fig. 2). Most of the freeze-dried solids showed glass transitions at temperatures close to or much higher than room temperature in the thermal analysis (Table 1). The absence of a crystal melting peak in the heating scan (*e.g.*, monosodium citrate: 217 °C) also indicated the limited excipient crystallinity in the co-lyophilized solids. Karl–Fischer titrimetry indicated a relatively high residual water content in the freeze-dried solids (Table 1). The high protein mass ratio was one likely reason for the high residual water content in the solids freeze-dried without the organic acid salts.

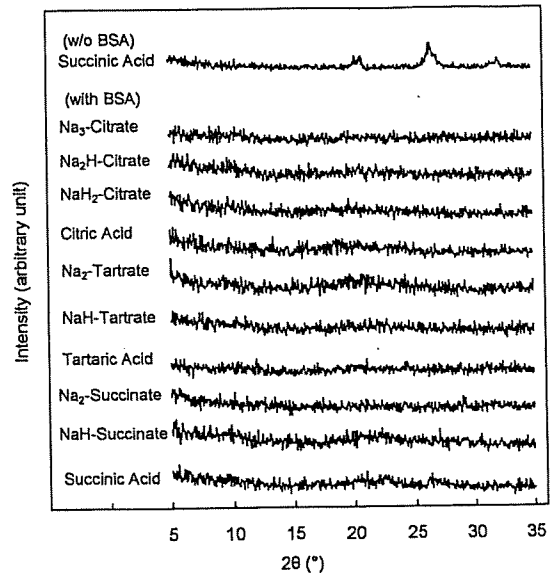

Fig. 2. Powder X-Ray Diffraction (XRD) Patterns of Excipients (50 mM) Freeze-Dried with or without BSA (10 mg/ml) and Corresponding Buffer Salts (1.5 mM)

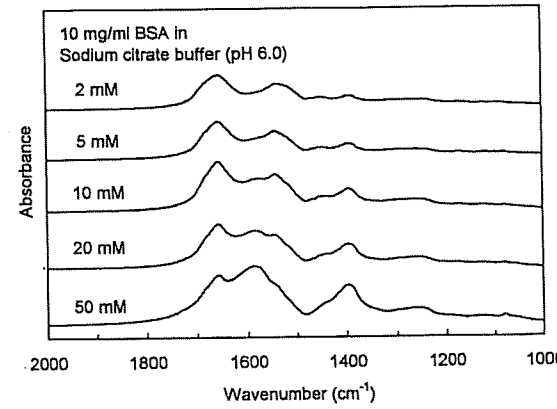

Fig. 3. FT-IR Spectra of BSA Freeze-Dried from Solutions Containing the Protein (10 mg/ml) and Various Concentrations (1.5—50 mM) of Sodium Citrate Buffer (pH 6.0)

FT-IR analysis was performed to elucidate the effect of buffer salts on the lyophilization-induced protein conformation change.[2,24,25] The following experiments were performed at certain (2—50 mM) buffer salt concentrations because of their overlapping absorbance in the co-lyophilized protein amide I band region (1600—1700 cm^{-1}) (Fig. 3). Figure 4 shows area-normalized second-derivative amide I spectra of BSA in solids freeze-dried from four buffer systems (20 mM, sodium phosphate, sodium citrate, sodium L-tartrate, sodium succinate, pH 6.0). A spectrum of the protein in its initial aqueous solution (10 mg/ml, 20 mM sodium citrate buffer, pH 6.0) was also included for comparison. The protein showed practically identical spectra in the four buffer solutions studied (Fig. 5). Freeze-drying of the protein from the buffer systems resulted in a varied extent of the lyophilization-induced structural perturbation as observed in the broad amide I spectra and reduced α-helix band (1656 cm^{-1}) intensity.[2,24,28—30] Larger structural changes were suggested in freeze-drying of the protein from sodium phosphate and sodium succinate buffer solutions.

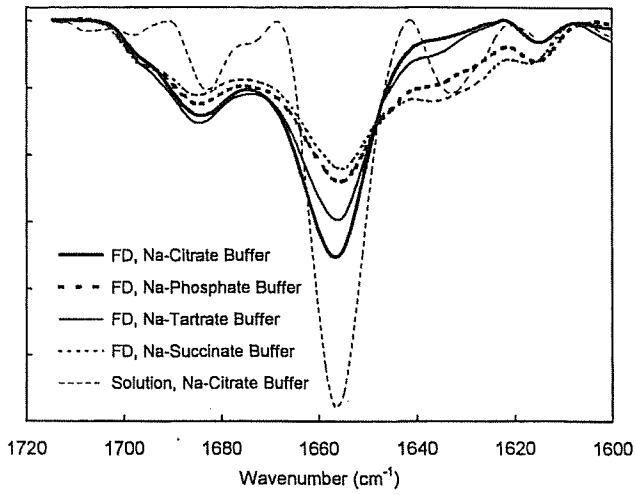

Fig. 4. Area-Normalized Second-Derivative Amide I Spectra of BSA Freeze-Dried from Solutions Containing the Protein (10 mg/ml) in Various Buffer Systems (20 mM, pH 6.0)

Fine dotted line denotes second-derivative spectra of BSA in the aqueous sodium phosphate buffer solution.

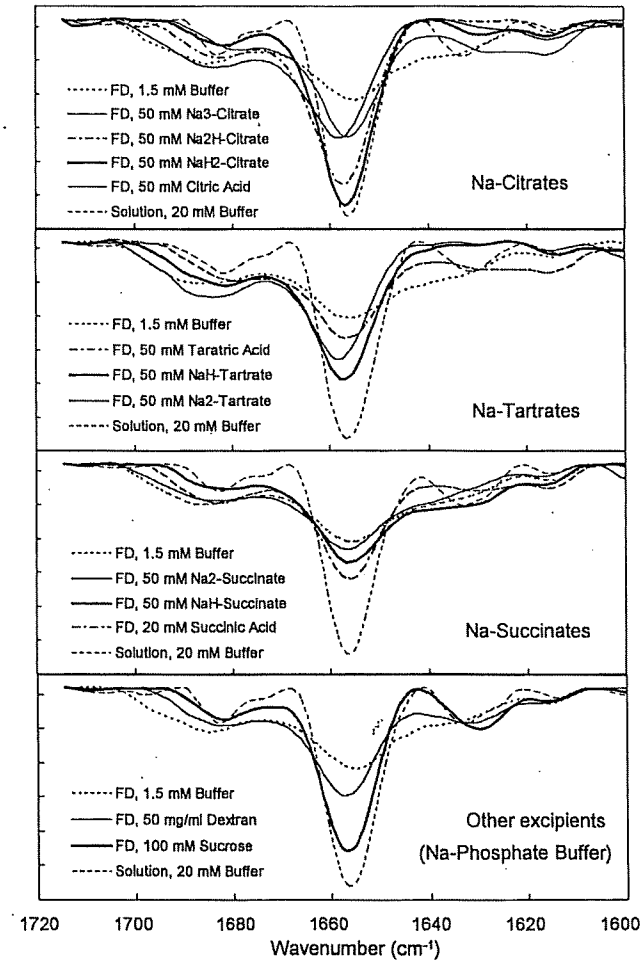

Fig. 5. Area-Normalized Second-Derivative Amide I Spectra of BSA Freeze-Dried from Aqueous Solutions Containing the Protein (10 mg/ml), Buffer Salts (1.5 mM), and Excipients (50 mM)

Fine dotted line denotes second-derivative spectra of BSA in the corresponding buffer solutions.

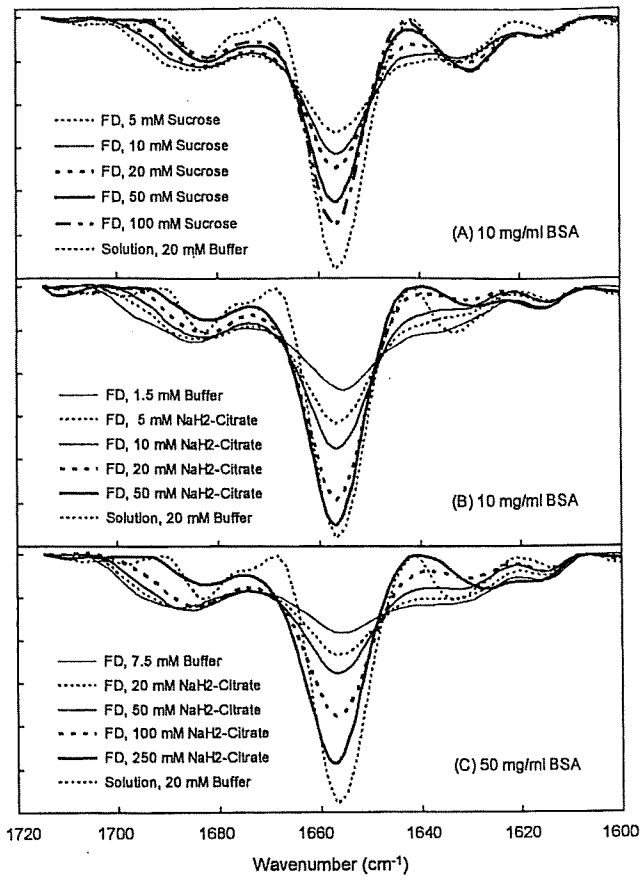

Fig. 6. Effect of Co-solutes on the Area-Normalized Second-Derivative Amide I Spectra of BSA Lyophilized at Different Concentrations (A, B: 10 mg/ml, C: 50 mg/ml).

Figure 5 shows area-normalized second-derivative amide I spectra of BSA freeze-dried with the organic acids and their salts (50 mM). Spectra of the protein in the corresponding buffer solutions (20 mM, pH 6.0) are also included. Freeze-drying of BSA (10 mg/ml) with the low concentration buffer components (1.5 mM) induced similar substantial structural changes. Monosodium citrate (50 mM) was most effective at retaining the large α-helix band that characterized the native protein structure upon freeze-drying. The spectra of BSA lyophilized at different concentrations (10, 50 mg/ml, Fig. 6) suggested the structure stabilized by monosodium citrate, which effect depended roughly on the salt/protein mass ratios. The α-helix band intensity reached a plateau at the salt concentrations (20—50 mM) lower than that of sucrose. Further addition of the salt induced a broader α-helix band presumably because of the overlapping absorbance (data not shown).

Other salts showed varied effects on the freeze-dried protein structures (Fig. 5). Disodium citrate and monosodium L-tartrate allowed BSA to retain its secondary structure to a lesser extent upon freeze-drying, compared to monosodium citrate. Trisodium citrate and citric acid were less effective at protecting the protein structure. Other organic acids and their salts showed a limited ability to protect the native protein conformation upon freeze-drying. The effect of succinic acid was studied at a lower (20 mM) concentration because of the large overlapping absorbance in the amide I region. Insuffi-

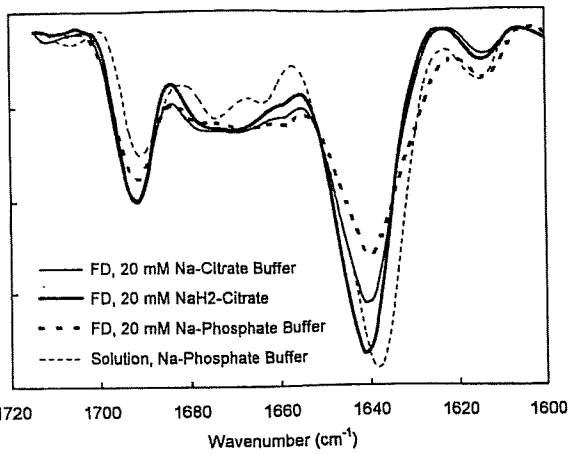

Fig. 7. Area-Normalized Second-Derivative Amide I Spectra of Immunoglobulin G in an Aqueous Buffer Solution (10 mg/ml) and Freeze-Dried Solids.

The initial monosodium citrate solution (20 mM) also contained a lower (10 mM) concentration of sodium citrate buffer salts.

cient intermolecular interaction with co-lyophilized protein due to steric hindrance should explain the lower structure-stabilizing effect of dextran 10.2k compared to sucrose.[31] No apparent relationship between the structure-stabilizing effect and the glass transition temperatures (T_g) or residual water content of the freeze-dried solid (Table 1) was observed.

Second-derivative amide I spectra of bovine IgG showed predominant intramolecular (1637 cm^{-1}) and intermolecular (1692—1695 cm^{-1}) β-sheet bands (Fig. 7). The reduced intramolecular β-sheet band intensity indicated that IgG freeze-dried from sodium phosphate buffer (20 mM, pH 6.0) had a partially altered structure. Monosodium citrate (50 mM) allowed the IgG to retain the intramolecular β-sheet band upon freeze-drying. Retention of the predominant bands at different wavenumbers strongly suggested the effect of salt to stabilize native protein conformation rather than an artifact induced by the overlapping absorption.

Discussion

The results indicate that some organic acid salts form glass-state amorphous solids that protect proteins from structural change during freeze-drying. The carboxylic acids and their sodium salts showed varied physical properties in the frozen solutions and their dried solids.[4] A network of rigid carboxyl/carboxylate interaction and hydrogen bonds should explain the high glass transition temperature of the lyophilized amorphous sodium citrate solids.[32,33] Our previous study also showed contribution of rigid molecular interactions to form glass-state solids by co-lyophilization of citric acid an L-arginine.[34] Many protein solutions have their T_g' at temperatures (approx. −10 °C) higher than those of smaller molecules.[27] The addition of proteins should reduce the mobility of other solute molecules in the freeze-concentrated phase, and thus prevent eutectic solute crystallization.

Freeze-drying of the protein in the sodium phosphate (20 mM) or lower concentrations of the carboxylic acid buffers (1.5 mM) perturbed their secondary structure. The structurally perturbed molecules usually return to their native structure upon re-hydration, whereas misfolding and/or binding between exposed hydrophobic regions are major causes of the lyophilization-induced protein aggregation. The structurally altered protein molecules are also prone to chemical degradation during storage.[1,2,24] Some glass-forming organic acid sodium salts (*e.g.*, sodium citrates) maintained the native secondary structure of co-lyophilized BSA and IgG. Such structural stabilization would explain the higher residual activity of proteins after freeze-drying from certain buffer systems.[12—16]

The organic acids should protect proteins through several mechanisms in the different physical states prior to and during the freeze-drying process. The fatty acid-poor BSA is most resistant to heat denaturation in weakly acidic to neutral (pH 5—7) solutions.[35] Freeze-drying of the protein in the region (pH 6.0) resulted in varied secondary structures depending on the buffer systems. Observed structural stabilization at certain salt/protein concentration ratios indicated the contribution of the direct interactions. It is highly plausible that the effective buffer salts provide proteins hydrogen bonds that substitute for those of the surrounding water molecules inevitable to retain the conformation. In addition, the lower effective concentration of monosodium citrate compared to sucrose suggested the contribution of electrostatic (ion–ion, ion–dipole) interactions between the salt anion (hydroxycarboxylate ion) and basic amino acid residues on protein surfaces for the structural stabilization.[17,36,37] The high T_g of the dried solids indicated mixing of the protein and salts required for the interaction. The topic of protein-stabilizing molecular interactions in the dried states, including the effect of differently ionized functional groups, will require further study for elucidation. The limited mobility of the surrounding molecules should prevent chemical degradation of the protein in glass-state solids. Similar structural (thermodynamic) and chemical (kinetic) stabilization of embedded proteins has been reported in disaccharides.[22,23] Some of the buffer components should also protect proteins from cold denaturation in the aqueous solutions and in the frozen solutions. The citrate^{3-} and L-tartrate^{2-} ions are 'kosmotropic' anions that thermodynamically stabilize native protein structures by being preferentially excluded from the immediate surface of the protein molecules.[16,17,22,38—41] In other words, the proteins are preferentially hydrated in the solute solutions.

The difference in the structure and physical properties would explain the varied protein-stabilizing effect of the organic acid salts through the above-mentioned mechanisms. Solution pH and anion structure are major factors that determine the thermal stability of proteins in aqueous carboxylic acid salt solutions.[17] Some di- and tricarboxylic acid salts protect proteins from thermal denaturation. The number of carboxyl and hydroxyl groups should is also likely to be important in protecting the secondary structure of BSA through the water-substituting hydrogen bonds and electrostatic interactions against the dehydration stress. The limited structure-stabilizing effect of succinic acid and its salts during freeze-drying, in spite of their apparent effect to improve the thermal stability of proteins in aqueous solutions, suggests that the hydroxyl group makes a large contribution to the structural stabilization against dehydration stresses. Possible salt crystallization at a higher salt/protein concentration ratio should further reduce the stabilizing interactions between them. Monosodium citrate should satisfy various requirements (*e.g.*, sufficient functional groups, appropriate ionized

states, propensity to form glass-state amorphous solids) for protein-stabilizing interactions in the dried states.

Our results emphasize the importance of choosing an appropriate buffer system when developing freeze-dried protein formulations. Salts that have a higher propensity for crystallization should be avoided especially at lower excipient/protein concentration ratios. Significant stabilizing effects of some organic acid salts are applicable to the design of sugar-free formulations. Some buffer components also raise the glass transition temperature of co-lyophilized disaccharide solids.[42,43] The retention of protein structural integrity in the amorphous salt solids would also be relevant to other applications of proteins in ionic environments, including enzyme reactions in ionic liquids (RTMS: room temperature molten salts).[44—46] Careful optimization of ingredients based on the physical and chemical properties of the excipients should ensure the optimal processing and storage stability of protein formulations.

Acknowledgements This work was supported in part by the Japan Health Sciences Foundation (KHB1006).

References

1) Chang B. S., Beauvais R. M., Dong A., Carpenter J. F., *Arch. Biochem. Biophys.*, **331**, 249—258 (1996).
2) Prestrelski S. J., Tedeschi N., Arakawa T., Carpenter J. F., *Biophys. J.*, **65**, 661—671 (1993).
3) Hermeling S., Crommelin D. J., Schellekens H., Jiskoot W., *Pharm. Res.*, **21**, 897—903 (2004).
4) Shalaev E. Y., Johnson-Elton T. D., Chang L., Pikal M. J., *Pharm. Res.*, **19**, 195—201 (2002).
5) MacKenzie A. P., *Bull. Parenter. Drug Assoc.*, **20**, 101—130 (1966).
6) Akers M. J., Vasudevan V., Stickelmeyer M., *Pharm. Biotechnol.*, **14**, 47—127 (2002).
7) Williams-Smith D. L., Bray R. C., Barber M. J., Tsopanakis A. D., Vincent S. P., *Biochem. J.*, **167**, 593—600 (1977).
8) Murase N., Franks F., *Biophys. Chem.*, **34**, 293—300 (1989).
9) Sarciaux J. M., Mansour S., Hageman M. J., Nail S. L., *J. Pharm. Sci.*, **88**, 1354—1361 (1999).
10) Pikal-Cleland K. A., Rodriguez-Hornedo N., Amidon G. L., Carpenter J. F., *Arch. Biochem. Biophys.*, **384**, 398—406 (2000).
11) van den Berg L., Rose D., *Arch. Biochem. Biophys.*, **81**, 319—329 (1959).
12) Hynes H. E., Owen C. A. J., Bowie E. J., Thompson J. H. J., *Blood*, **34**, 601—609 (1969).
13) Osterberg T., Fatouros A., Mikaelsson M., *Pharm. Res.*, **14**, 892—898 (1997).
14) Chang B. S., Reeder G., Carpenter J. F., *Pharm. Res.*, **13**, 243—249 (1996).
15) Labrude P., Vigneron C., *J. Pharm. Pharmacol.*, **32**, 305—307 (1980).
16) Busby T. F., Atha D. H., Ingham K. C., *J. Biol. Chem.*, **256**, 12140—12147 (1981).
17) Kaushik J. K., Bhat R., *Protein Sci.*, **8**, 222—233 (1999).
18) Li J., Chatterjee K., Medek A., Shalaev E., Zografi G., *J. Pharm. Sci.*, **93**, 697—712 (2004).
19) Arakawa T., Timasheff S. N., *Biochemistry*, **21**, 6536—6544 (1982).
20) Carpenter J. F., Crowe J. H., *Biochemistry*, **28**, 3916—3922 (1989).
21) Izutsu K., Yoshioka S., Terao T., *Pharm. Res.*, **10**, 1232—1237 (1993).
22) Carpenter J. F., Prestrelski S. J., Arakawa T., *Arch. Biochem. Biophys.*, **303**, 456—464 (1993).
23) Franks F., *Dev. Biol. Stand.*, **74**, 9—18 (1992).
24) Dong A., Prestrelski S. J., Allison S. D., Carpenter J. F., *J. Pharm. Sci.*, **84**, 415—424 (1995).
25) Susi H., Byler D. M., *Biochem. Biophys. Res. Commun.*, **115**, 391—397 (1983).
26) Kendrick B. S., Dong A., Allison S. D., Manning M. C., Carpenter J. F., *J. Pharm. Sci.*, **85**, 155—158 (1996).
27) Chang B. S., Randall C., *Cryobiology*, **29**, 632—656 (1992).
28) Carter D. C., Ho J. X., *Adv. Protein Chem.*, **45**, 153—203 (1994).
29) Murayama K., Tomida M., *Biochemistry*, **43**, 11526—11532 (2004).
30) Luthra S., Kalonia D. S., Pikal M. J., *J. Pharm. Sci.*, **96**, 2910—2921 (2007).
31) Kreilgaard L., Frokjaer S., Flink J. M., Randolph T. W., Carpenter J. F., *J. Pharm. Sci.*, **88**, 281—290 (1999).
32) Kadoya S., Izutsu K., Yonemochi E., Terada K., Yomota C., Kawanishi T., *Chem. Pharm. Bull.*, **56**, 821—826 (2008).
33) Inabe T., *J. Mater. Chem.*, **15**, 1317—1328 (2005).
34) Izutsu K., Kadoya S., Yomota C., Kawanishi T., Yonemochi E., Terada K., *Chem. Pharm. Bull.*, **57**, 43—48 (2009).
35) Gumpen S., Hegg P. O., Martens H., *Biochim. Biophys. Acta*, **574**, 189—196 (1979).
36) Tian F., Middaugh C. R., Offerdahl T., Munson E., Sane S., Rytting J. H., *Int. J. Pharm.*, **335**, 20—31 (2007).
37) Izutsu K., Fujimaki Y., Kuwabara A., Aoyagi N., *Int. J. Pharm.*, **301**, 161—169 (2005).
38) Arakawa T., Timasheff S., *Biochemistry*, **23**, 5912—5923 (1984).
39) Hofmeister F., *Arch. Exp. Pathol. Pharmakol.* (Leipzig), **24**, 247—260 (1888).
40) Jensen W. A., Armstrong J. M., Giorgio J. D., Hearn M. T., *Biochim. Biophys. Acta*, **1296**, 23—34 (1996).
41) Ru M. T., Hirokane S. Y., Lo. A. S., Dordick J. S., Reimer J. A., Clark D. S., *J. Am. Chem. Soc.*, **122**, 1565—1571 (2000).
42) Ohtake S., Schebor C., Palecek S. P., de Pablo J. J., *Pharm. Res.*, **21**, 1615—1621 (2004).
43) Kets E. P., IJpelaar P. J., Hoekstra F. A., Vromans H., *Cryobiology*, **48**, 46—54 (2004).
44) Fujita K., MacFarlane D. R., Forsyth M., *Chem. Commun.* (Camb.), **2005**, 4804—4806 (2005).
45) van Rantwijk F., Madeira L. R., Sheldon R. A., *Trends Biotechnol.*, **21**, 131—138 (2003).
46) Ohno H., *Bull. Chem. Soc. Jpn.*, **79**, 1665—1680 (2006).

バイオ後続品とは　ー開発状況と規制についてー

川西　徹[1]

要旨：　国際的にバイオ医薬品後発品（バイオ後続品）の開発が活発化し、規制の枠組みの構築が行われつつある。バイオ後続品は後発医薬品と異なり、先発バイオ医薬品との同等・同質性を示すために、品質特性評価データに加えて、通常非臨床・臨床試験データが必要とされる。したがって従来の後発医薬品と異なる規制の枠組みが必要である。欧州はいち早く規制体制を確立し、既に約10の製品が承認されている。我が国においても開発が活発化しており、承認された製品はまだないが、バイオ後続品ガイドラインが近々に公表される予定であり、広く臨床で使用されるようになると思われる。

1．今なぜバイオ医薬品後発品が注目されるのか？

バイオ医薬品は1982年に米国でヒトインスリンを第一号として認可され、その後様々な製品が開発され、世界各国で認可、臨床で広く使用されている。現在、バイオ医薬品の後発品が話題となっている第一の理由は、これらの製品の中で2001年から特許の期限を迎える製品があり、その数は年々増えており、後発品開発の対象となったことである[1-2]。タンパク質性医薬品の場合、分子量の小さい化学合成薬品のように構造が判っていれば容易に製造できるという訳ではない。しかしながら、欧米の後発品メーカー、あるいはアジア諸国の製薬企業を中心に、バイオ医薬品の後発品開発の機運が高まっている。第二の理由としては、先進国における医療費高騰があげられる。先進国においては、高齢化も相まって医療費の高騰が社会経済的に大きな負担となっており、医療費の中で大きな割合を占める薬剤費の節約は医療費削減に向けた大きな目標となっている。一方発展途上国においては、多くのバイオ医薬品は高額ゆえに患者さんのもとに届きにくいという事情もある。このような背景の中、欧米では既にいくつかの製品が認可をうけており、さらにアジア諸国の中には、既に多くの製品が認可されている国がある。一方、我が国においても、特許が切れた製品が増えるにつれ、開発の機運が高まっており、既に承認申請されているものもあり、開発途上にある製品は少なくない。

2．バイオ医薬品の後発品は「バイオ後続品」

化学合成医薬品の場合、独占的販売期間（特許期間や再審査期間）を過ぎると先発医薬品企業以外の製薬企業が、後発医薬品として製品開発を行い、安い価格で販売する制度が社会的に受け入れられている。後発医薬品の条件としては、(1)先発品と有効成分が同一であり、(2)先発品と同一用法・用量の投与で、同一の効能・効果を示す、ということである。化学合成医薬品の後発品を承認申請するにあたっては、開発企業は (1)有効成分の同一性、

[1] 国立医薬品食品衛生研究所薬品部　部長（かわにし　とおる）